1995ApJ...441...28H

THE ASTROPHYSICAL JOURNAL, 441:28–50, 1995 March 1
© 1995. The American Astronomical Society. All rights reserved. Printed in U.S.A.

THE LARGE-SCALE DISTRIBUTION OF LATE-TYPE GALAXIES BETWEEN VIRGO AND THE GREAT WALL

G. LYLE HOFFMAN
Department of Physics, Lafayette College, Easton, PA 18042-1782
B. M. LEWIS
Arecibo Observatory, P.O. Box 995, Arecibo, PR 00613
AND
E. E. SALPETER
Center for Radiophysics and Space Research, Cornell University, Ithaca, NY 14853
Received 1994 April 4; accepted 1994 September 9

ABSTRACT

Neutral hydrogen data are presented for 88 of the Virgo Cluster Catalog galaxies thought on morphological grounds to lie in the background of the cluster. We confirm that the morphological assignment of cluster membership works quite well; very few of the "background" galaxies are in fact at cluster redshifts. The resulting sample of redshifts, along with optical redshifts from the literature, allow us to explore the large-scale distribution of galaxies in the space between the Local Supercluster and the Great Wall. Galaxies in a larger window around the Virgo Cluster, but at redshifts between Virgo and the Great Wall, have a fairly low average number density, but the distribution is far from uniform: Some portions resemble voids, but in other portions galaxies can be assigned to clouds or filaments of appreciable size (sometimes containing bound groups). We investigate the luminosity function in high- and low-density regions of our galaxy sample, which excludes the Virgo Cluster proper. We find no significant difference. However, our selection procedures are insensitive to galaxies of *very* low surface brightness, which have been reported to be more abundant in low-density regions.

The average probability of a line of sight intersecting the optical disk of our sample galaxies is derived separately for the Virgo Supercluster region (redshifts below 3500 km s^{-1}) and for the region behind (out to 10,000 km s^{-1}). The number density ratio of Lyα forest lines to galaxies is larger by a factor of order 10 in the far (low-density) region than in the near. A survey of recent literature on galaxy redshifts uncovers a new candidate, MCG 0-32-16, for the lowest redshift absorption line.

Subject headings: galaxies: clusters: individual (Virgo) — galaxies: distances and redshifts — quasars: absorption lines — radio lines: galaxies

1. INTRODUCTION

Much attention has been given in recent studies to the Virgo cluster of galaxies, with its extended Local Supercluster (de Vaucouleurs & Corwin 1986; de Vaucouleurs & Peters 1985; Tully & Shaya 1984; Tully 1987; Tully, Shaya, & Pierce 1992; Tanaka 1985a, b; Binggeli, Tammann, & Sandage 1987; Binggeli, Popescu, & Tammann 1993; Hoffman et al. 1989a, b; Han & Mould 1990; Pellegrini & da Costa 1990; Sandage & Tammann 1990; Dressler 1991; Shimasaku & Okamura 1992; Teerikorpi et al. 1992; Fukugita, Okamura, & Yasuda 1993; Jerjen & Tammann 1993; and references in each) and to the more distant Coma cluster in its Great Wall (Gavazzi & Trinchieri 1989; Gavazzi, Garilli, & Boselli 1990; Salzer, Hanson, & Gavazzi 1990; Karachentsev & Kopylov 1990; Lucey et al. 1991; Ramella, Geller, & Huchra 1992; Thompson & Gregory 1993; and references in each). The more sparsely populated regions between have received much less attention (Hoffman 1989; Binggeli et al. 1993, hereafter BPT).

In compiling the Virgo Cluster Catalog (hereafter VCC), Binggeli, Sandage, & Tammann (1985, hereafter BST) relied primarily on a morphological evidence to determine whether galaxies are members of the Virgo Cluster, background galaxies, or members of the complex of groups (W and M in particular) in the near background, 70% or so more distant than the cluster (BST called these "possible members" of Virgo). Our redshift survey (Hoffman et al. 1987, 1989b, c) of the spiral and dwarf irregular galaxies designated as cluster members or possible members showed that, except for the mixed bag of "blue compact dwarf" (hereafter BCD) galaxies (Hoffman et al. 1989a), the morphological assignment of cluster members was quite accurate, only a handful of galaxies so assigned having redshifts $\gtrsim$3000 km s^{-1} as discussed by BPT. One open question is the converse: how accurate was the BST morphological assignment to the background? Are any significant numbers of those galaxies in fact cluster members? Our Arecibo[1] H I 21 cm observations of most of the BST "background" galaxies are reported in § 2.

One question left open by the studies of the populous regions is the connection between the Local Supercluster and the Great Wall: are they distinct entities, completely severed from one another by a virtual void of galaxies, or is there a filamentary connection? In § 3 we perform a percolation analysis on the galaxies behind and around the Virgo Cluster to investigate the connection, and to assign galaxies to clouds or associations likely to be at a common distance for eventual Tully-Fisher analyses.

[1] The Arecibo Observatory is part of the National Astronomy and Ionosphere Center, which is operated by Cornell University under a management agreement with the National Science Foundation.

© American Astronomical Society • Provided by the NASA Astrophysics Data System

1995ApJ...441...28H

The nature and morphological composition of any small groups and the general field that lie in the void are also of interest in view of theoretical questions (Dekel & Silk 1986; Tyson & Scalo 1988; Lacey & Silk 1991; Babul & Rees 1992; Salpeter 1993) as to whether the galaxy distribution is biased, with dwarf galaxies and/or galaxies of low surface brightness more prominent in the voids than in rich clusters. We discuss the luminosity function of our sample of galaxies and its dependence on local density in § 4.

Perhaps the most compelling reason to study the large-scale distribution of late-type galaxies in the background of Virgo is the discovery by Bahcall et al. (1991) and Morris et al. (1991) of low column density Lyα absorption lines in the spectrum of 3C 273, ranging in redshift from 1050 km s^{-1} on up to the redshift of the QSO itself. In § 5 we combine our results with other redshift compilations in the literature to discuss the relation between galaxy grouping or individual galaxy disks and Lyα absorption lines. Such a discussion has to consider three different length scales:

I. On scales of 10 to 50 Mpc (and velocity differences of a few thousand km s^{-1}), there is a very marked contrast between giant superclusters and giant voids in some directions on the sky, and a slightly less marked (but more typical) contrast within about 20° of the 3C 273 line of sight. The region between the Local (Virgo) Supercluster and the Great Wall is a "semivoid," with a medium-low average number density of galaxies, which contains galaxy groups (and "clouds of groups") scattered through large regions of very low density. We derive two numbers relevant to the large scales: separately for the high-density (Virgo) region out to $V \sim 3500$ km s^{-1} and the low-density region $3500 \lesssim V \lesssim 10{,}000$ km s^{-1}, we find the average probability (averaged over about 20°) that a line of sight intersects the optical disk of a late-type galaxy. This will give the factor (appreciably larger for the low-density region than for the supercluster) by which the optical disk area has to be multiplied if extended hydrogen disks of ordinary, visible, disk galaxies were to provide all the Lyα "forest" lines.

II. The galaxy groups have sizes of 1 to a few Mpc and several hundred km s^{-1}, but our percolation analysis also identifies "clouds of groups" or "filaments" with sizes of order 10 Mpc.

III. Absorbing systems directly associated with individual galaxies would have velocity differences of $\sim$100 or 200 km s^{-1}. We defer discussion of the probability that individual galaxy disks contribute to the observed absorption lines to a companion paper (Salpeter & Hoffman 1995).

Section 6 presents a summary and conclusions.

2. OBSERVATIONS

A number of VCC background galaxies (BST) were observed in the course of our surveys of H I in the spiral and dwarf irregular members of the Virgo Cluster (Helou et al. 1981; Helou, Hoffman, & Salpeter 1984; Hoffman et al. 1987, 1989b, c, hereafter collectively HS et al.). In several observing sessions between 1987 and 1992, we sought to extend the survey to all 137 spiral ($T \geq 3$) galaxies classified as "background" in the VCC. Due to time constraints, we have been able to obtain data for only 88 of the galaxies, with eight of those being undetected in the redshift range 0–8000 km s^{-1} Of the remaining 49, 20 have optical redshifts available in the VCC. In all, 37 of the 137 galaxies have redshifts unknown at this writing. We also observed and detected an additional 12 galaxies that lie outside the VCC survey boundary.

We used the 22 cm dual circular system at Arecibo throughout. Our procedure varied, depending on whether or not an optical redshift was available in the VCC. For galaxies with known redshift, we used frequency-switched observations with the galaxy's signal in both frequency buffers to make more efficient use of telescope time. For galaxies without known redshift, we performed redshift searches using ON/OFF total power pairs with quadrants of the autocorrelator shifted by 7.5 MHz to cover a total velocity range of 8000 km s^{-1} in each scan. If necessary, additional scans were acquired spanning higher velocity intervals up to about 16,000 km s^{-1}. The fluxes were calibrated by observing continuum sources from the catalog of Bridle et al. (1972) or the NRAO calibrator list.

The data were reduced using the NAIC ANALYZ data reduction package, correcting for zenith angle and the frequency sensitivity of the feed in the usual manner (see, e.g., Haynes & Giovanelli 1984). Hanning-smoothing was applied so that our final velocity resolution is about 15 km s^{-1}, with rms sensitivity 2 mJy or less. From the profiles, we obtained profile widths ΔV_{50} and ΔV_{20} at 50% and 20% of the nearest peak, measured outward, integrated fluxes $\int S dV$ and heliocentric systemic velocities $v_\odot$ taken to be the midpoint of the two edges at 50% of the nearest peak. Uncertainties in the velocities and profile widths follow the prescription of Schneider et al. (1986); uncertainties in the fluxes are typically 10%.

Our results for detected galaxies are given in Table 1, which is organized as follows: Column (1) gives a common name by which the galaxy is known. NGC refers to Dreyer (1888), and IC to Dreyer (1895, 1908) as usual; UGC refers to Nilson (1973; CGCG refers to Zwicky, Herzog, & Wild (1961–1963); and VCC refers to the Virgo Cluster Catalog of BST. The galaxy's (epoch 1950) right ascension (in hhmmss.s format) and declination (in ddmmss format) appear in column (2) (upper and lower lines, respectively). Column (3) holds the morphological type as coded by BST. The blue magnitude in column (4) (*upper line*) is taken from BST or RC3 (de Vaucouleurs et al. 1991), as is the isophotal diameter in the lower line; we have substituted BST's estimated diameter when log D_{25} is not available. The heliocentric systemic velocity $v_\odot$, in km s^{-1}, from our H I profiles is shown in the upper line of column (5) along with its standard 1 σ uncertainty in the lower line; for comparison, the velocity listed in VCC (when available) and the optical velocity from RC3 are given in the upper and lower lines, respectively, of column (6). The H I profile widths at 50% and 20% follow in column (7)'s upper and lower lines, respectively. Both are in km s^{-1}. The flux integral, in Jy km s^{-1}, and rms noise, in mJy, in the signal-free parts of the spectrum appear in column (8). Finally, an asterisk in column (9) indicates that there is a note about the galaxy in the following paragraphs. The individual spectra are shown in Figure 1.

Notes on individual entries in Table 1 follow.

IC 3008.—Our results are consistent with those of Williams & Kerr (1981) but have higher signal to noise ratio.

PGC 3863.—Gordon & Gottesman (1981) report $\Delta V = 205$ km s^{-1}, much narrower than our profile, and a flux smaller than ours by a factor of 2. Their position differs from ours by 22″, not large enough to account for the difference. Their spectrum has somewhat lower signal to noise ratio than ours; we suspect that the difference lies in a misidentification of the profile edge.

© American Astronomical Society • Provided by the NASA Astrophysics Data System

1995ApJ...441...28H

TABLE 1

DETECTED GALAXIES[a]

Name	RA Dec.	Type	B_T $\log D_{25}$	$V_\odot$ σ	V_{VCC} V_{RC3}	ΔV_{50} ΔV_{20}	$\int SdV$ rms	Note
(1)	(2)	(3)	(4)	(5)	(6)	(7)	(8)	(9)
NGC 4012	115553.1	Sb	14.25	4182		382	5.5	
	101800		1.29	2		407	1.1	
CGCG 069-034	120102.1	...	14.47	6053		274	1.2	
	84000		...	5		300	0.7	
CGCG 069-038	120145.7	...	14.43	10289		346	1.4	
	90513		...	4		376	0.4	
PGC 38304	120308.3	S?	15.3	10208		323	10.5	
	91607		0.82	2	6377	361	1.9	
IC 3008	120522.7	S?	14.94	6977		343	4.6	*
	135048		0.94	2		371	0.9	
PGC 38634	120700.0	S?	14.54	6714		304	0.63	*
	171713		1.04	6	6660	320	0.7	
VCC 12	120711.0	SBa(s)	15.3	8660		430	1.6	
	122406		0.95	4		450	0.8	
VCC 28	120812.6	SBc	15.38	6325		189	0.92	
	160842		0.91	11		219	1.4	
UGC 7196	120926.3	Sbc (on edge)	15.09	7094	7095	660	1.3	*
	154054		1.13	11		714	0.5	
VCC 40	120930.0	Sbc(s)	15.38	6949		401	1.2	*
	151106		0.97	4		413	1.3	
UGC 7210	120958.1	Sb (on edge)	15.24	7072	7137	500	1.6	*
	153300		0.93	29		505	1.5	
IC 3039	120959.3	Sc	15.37	7642	7001	347	1.6	*
	123512		0.99	5		368	1.2	
UGC 7230	121106.0	Sc+Sc	14.51	7127	7133	76	5.4	*
	162406		1.15	1	7128	142	1.3	
NGC 4186	121133.5	Sa(r)	14.65	7882		327	1.1	*
	150018		1.04	5		340	1.2	
IC 3060	121230.0	Sab	14.64	5826	5808	277	2.9	*
	124800		1.10	4		293	1.8	
UGC 7273	121311.0	Sbc(s)II	15.36	11117	11223	491	3.9	
	82442		0.98	3	11223	511	1.2	
IC 3079	121331.1	SBa (smooth)	15.2	7974	8077	105	0.80	
	114842		0.86	27		402	1.0	
VCC 186	121348.5	Sa (on edge)	15.1	6318	6280	412	1.2	
	110500		0.95	5		423	1.3	
IC 3107	121514.2	Sbc(s)I-II	14.22	7289	7292	415	5.9	*
	110723		1.14	3	7299	450	1.2	
IC 3111	121518.0	Sb(s)II	14.78	14755	14793	449	0.72	
	84230		0.86	11		459	0.8	
VCC 262	121522.1	Sc(s)II	15.1	6991		231	2.0	
	60900		0.95	13		288	2.1	
UGC 7336	121532.3	Sc	15.47	6861	6852	320	1.6	*
	161430		0.97	4		331	1.7	
IC 3127	121602.4	Sbc(s)I-II	15.13	7457	8688	758	4.6	*
	120854		0.80	42		865	1.7	
VCC 297	121605.4	Sc (on edge)	15.1	1999		164	1.5	
	65906		1.16	3		188	1.0	
IC 3128	121609.0	Sc (tides)	15.19	11629	11680	419	2.3	
	120030		0.81	12	11623	462	1.3	
VCC 331	121642.0	pec	15.0	1984		84	0.56	*
	63418		0.89	7		106	2.0	
IC 3151	121700.0	SBa(r)I	14.63	7424	7377	410	1.3	
	94136		1.03	7		442	0.8	
IC 3156	121711.4	SBc(s):	14.51	5876	5784	216	1.7	
	92536		0.91	3		258	1.2	
UGC 7383	121728.8	Sbc(r)I.2	14.56	7376	7374	287	5.0	*
	85254		1.01	1		309	1.2	
VCC 392	121733.0	SBc(r)I	14.91	19390	19336	387	1.4	
	80524		0.73	13		425	1.3	
VCC 395	121736.6	Sc(s)II	14.60	7382	7388	344	3.6	
	85518		1.16	4		365	1.7	

© American Astronomical Society • Provided by the NASA Astrophysics Data System

1995ApJ...441...28H

TABLE 1—*Continued*

Name	RA Dec.	Type	B_T $\log D_{25}$	$V_\odot$ σ	V_{VCC} V_{RC3}	ΔV_{50} ΔV_{20}	$\int SdV$ rms	Note
(1)	(2)	(3)	(4)	(5)	(6)	(7)	(8)	(9)
VCC 406	121746.0	SBbc(r) pec	15.00	4424		84	0.92	
	84836		0.75	2		104	1.2	
IC 3174	121756.4	Sb(r)I	15.04	9518		327	1.6	
	103124		1.03	5		338	1.3	
IC 3175	121800.5	Sb(r)II	16.04	5892	5904	354	2.2	*
	100754		0.71	4		373	1.3	
NGC 4287	121815.5	S (on edge)	14.65	2155		228	1.4	
	55506		1.26	3		239	1.7	
IC 3188	121822.0	Sbc(s)II	15.26	5898	5877	272	1.8	
	111712		0.78	4	5402	298	1.2	
IC 3209	121934.0	Sbc(s)I-II	15.71	7518	7521	423	1.1	*
	120200		0.88	14	7531	454	1.0	
VCC 568	122006.5	S (on edge)	14.91	2838		100	0.96	
	63006		1.10	9		159	1.9	
NGC 4326	122038.5	SBa(r)	14.19	7120	7112	307	1.5	
	62100		1.17	3	7128	318	1.4	
IC 3244	122040.1	Sc(s)II	15.04	12714	12836	301	2.4	
	143954		0.88	3	12880	332	1.2	
NGC 4333	122049.8	SBab(s)	14.48	7040	6975	117	1.03	
	61854		0.95	9	7002	207	1.2	
IC 3255	122103.0	Sbc(s)II	14.6	6480	6460	142	1.6	
	95454		0.76	7		216	1.2	
UGC 7464	122109.0	Sc(s)	15.14	7546		499	4.8	
	31412		1.15	3		513	1.7	
VCC 690	122128.7	S (on edge)	15.23	7017		250	1.5	
	53524		1.10	4		264	1.5	
IC 3271	122142.0	Sc(r)I	14.53	7209	7212	156	2.3	*
	81342		1.00	3		177	1.6	
VCC 729	122155.0	Sbc(r)I-II	15.03	7638	7624	234	2.6	*
	133036		0.95	2		246	1.7	
VCC 734	122200.0	SBbc(s)	15.1	5631		169	2.6	
	65918		0.80	2		189	1.3	
IC 787	122254.0	Sa	15.20	9257	9225	639	1.06	
	162400		1.03	22	9225	673	1.4	
VCC 822	122307.2	SBc	15.04	6898		244	1.3	*
	91136		0.86	4		266	1.2	
VCC 822a	122307.2	...	...	7135		66	0.26	*
	91136		...	7		86	1.2	
IC 3327	122327.5	SBa	15.02	13161	13222	300	0.59	*
	150948		0.80	30		314	0.9	
VCC 908	122357.5	Sc	14.82	7454	7470	245	0.98	*
	82012		0.86	44		479	1.3	
IC 3357	122418.5	Sc:	15.2	14084	13697	411	1.3	*
	100330		0.73	6		428	1.2	
IC 792	122437.1	Sc(s)II	14.80	6222	6205	367	4.6	*
	163618		1.20	2		387	1.4	
NGC 4432	122500.0	Sc(s)I-II	14.82	6402	6466:	166	5.1	
	63030		0.97	1	6403	188	1.7	
VCC 1058	122528.7	S (on edge)	15.3	4190		260	1.4	*
	43406		0.86	28		318	1.9	
VCC 1084	122541.3	Sb pec	14.9	7421	7401	114	0.83	
	75306		0.86	2		127	1.3	
VCC 1152	122627.5	Sb(r)II	14.82	7454	7478	341	0.54	*
	80742		1.03	40		349	1.3	
VCC 1206	122705.4	SBc(s)II	14.81	7355	7300	200	0.61	
	94630		0.86	7		221	1.0	
IC 3425	122723.3	Sb(s)I-II	14.60	7318	7361	391	4.8	
	105318		1.21	2		417	1.2	
IC 3432	122755.7	Sc	15.46	5960	6023	369	1.4	*
	142606		0.78	28	6019	422	1.1	
IC 3467	122952.1	Sc	15.28	7506	7559	277	8.9	
	120348		1.03	3	7560	315	1.9	

© American Astronomical Society • Provided by the NASA Astrophysics Data System

1995ApJ...441...28H

TABLE 1—*Continued*

Name	RA Dec.	Type	B_T $\log D_{25}$	$V_\odot$ σ	V_{VCC} V_{RC3}	ΔV_{50} ΔV_{20}	$\int SdV$ rms	Note
(1)	(2)	(3)	(4)	(5)	(6)	(7)	(8)	(9)
IC 3484	123034.1	Sc(s)I	14.89	8015	8045	285	2.2	
	174048		0.92	3		304	1.1	
VCC 1504	123054.0	Sc	15.0	7295	7270	207	1.5	
	133024		0.56	7		237	1.6	
VCC 1525	123118.5	Sbc(r)II	14.81	11359	11381	100	1.2	
	81806		0.73	5		128	1.8	
IC 3500	123118.5	SBc	15.44	6121	6163	190	2.2	
	141430		0.80	2	6163	214	1.6	
IC 3505	123139.0	SBc	14.91	13835	13907	529	2.3	
	161500		1.07	14		568	1.6	
NGC 4538	123207.7	S pec	15.3	4673	5100	272	4.0	
	33554		0.83	4	5100	305	1.8	
IC 3528	123225.0	Sbc	15.24	13828	13780	244	1.4	
	155036		0.69	15	13764	353	1.0	
VCC 1636	123313.2	Sb(r)II	15.13	9172		341	2.0	*
	144118		1.03	3		376	2.1	
IC 3567	123351.0	Sbc(s)II	14.9	9159	9233	234	1.8	
	135248		1.07	6		266	1.4	
VCC 1748	123539.5	SBa(s)	15.79	11308	11333	362	1.2	
	80512		0.86	6		377	1.1	
NGC 4588	123613.2	Sc(s)I-II	14.98	5610		298	4.7	
	70242		1.10	3		327	1.6	
VCC 1774	123620.3	S	15.1	7167	7338	348	1.2	
	72324		0.76	7		359	0.8	
VCC 1802	123706.5	S	14.9	7251	7278	302	2.7	
	72636		0.76	7		351	1.4	
IC 3629	123715.0	Sbc	15.2	13915	13876	580	1.6	
	134830		1.01	50		717	1.2	
IC 3638	123749.7	Sbc(r)II	14.25	6461	6474	92	1.1	
	104612		0.95	3		110	1.8	
VCC 1838	123751.0	Sc	15.0	14006	14217	936	2.5	
	82654		0.95	8		944	1.4	
VCC 1908	123934.1	S pec	15.1	7048		159	1.7	
	54654		0.56	6		216	1.1	
IC 3690	124018.0	Sb:	15.18	7616	7610	368	2.3	*
	103800		1.04	10		413	1.1	
IC 3709	124132.0	Sbc(r)I-II	15.28	14310	14336	301	2.5	
	92012		0.83	4	14336	323	1.5	
IC 3724	124222.0	Sc(s)I-II	15.1	9444		944	4.8	
	103324		0.86	13		1001	1.3	
VCC 2018	124245.0	Sa	14.88	9034	9025	164	3.4	
	102754		1.16	1		186	1.3	
IC 3754	124343.7	SBa	14.60	6456	6463	463	3.2	*
	83718		1.09	3		478	1.2	
IC 816	124415.0	RSBa	14.86	7189	7132	148	0.49	
	100742		0.97	14	7038	174	1.5	
CGCG 043-024	124454.9	...	14.47	5268		155	0.77	
	31840		...	4		179	0.6	
VCC 2076	124604.0	SBbc	15.3:	7554		116	0.81	*
	92400		0.76	18		184	1.8	
UGC 8192	130348.0	Sab	14.0	9665		291	3.2	*
	103840		1.19	12		340	2.3	
UGC 8972	140112.0	Sb	14.58	11511	11338	508	4.5	*
	113727		1.08	2		525	0.9	
NGC 5519	141151.6	Sa	14.0	7454		370	4.0	*
	74457		1.21	3		400	1.0	
UGC 9134	141408.0	Scd*	14.8	11151		286	2.3	*
	101300		1.14	5		337	1.3	
UGC 9229	142204.2	SAB(rs)bc pec	...	11631		59	1.6	*
	12347		1.01	2		87	1.6	

[a] See text for explanation of columns.

© American Astronomical Society • Provided by the NASA Astrophysics Data System

1995ApJ...441...28H

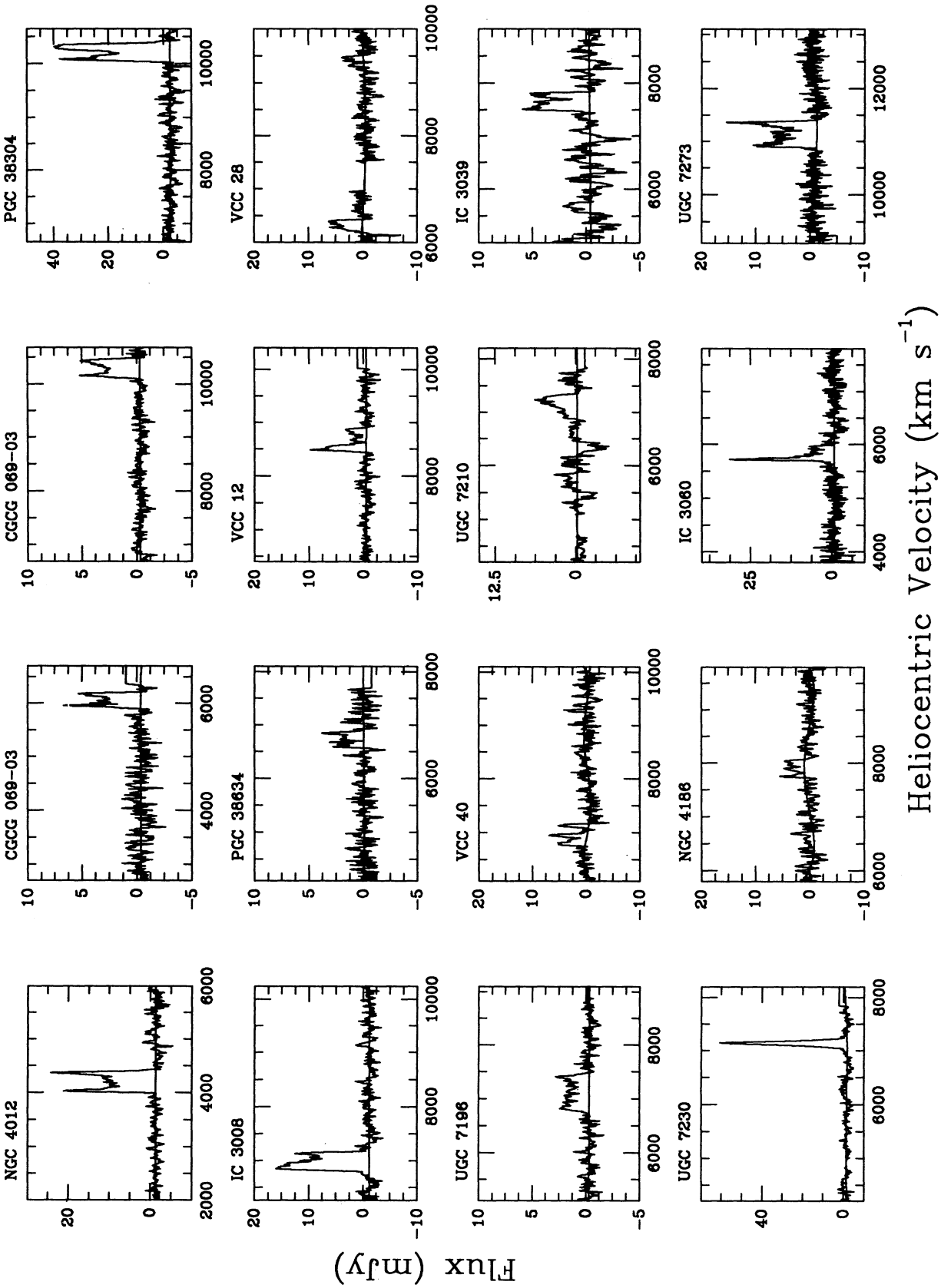

FIG. 1.—Spectra for each of the detected galaxies, in the order by which they appear in Table 1

© American Astronomical Society • Provided by the NASA Astrophysics Data System

1995ApJ...441...28H

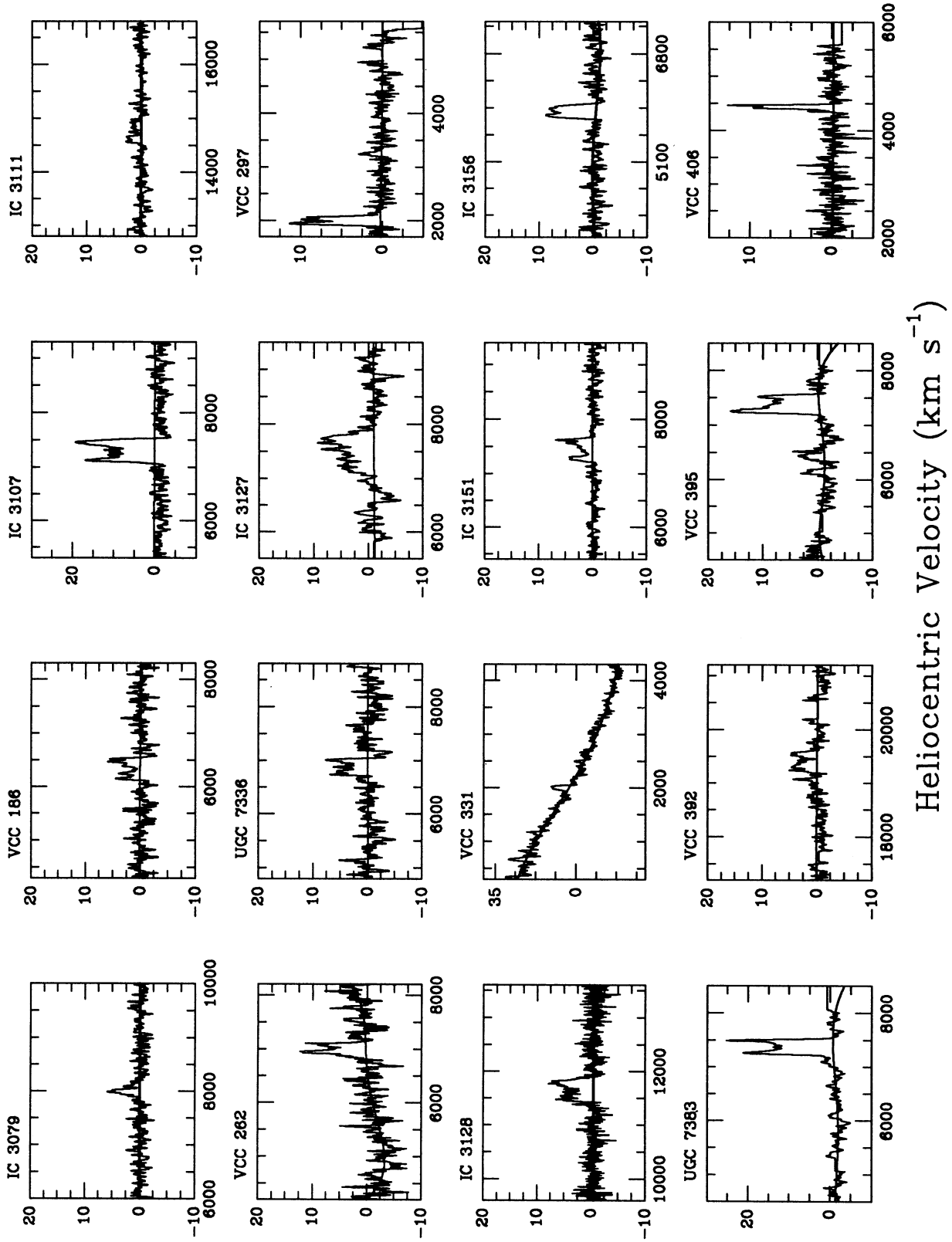

FIG. 1—*Continued*

© American Astronomical Society • Provided by the NASA Astrophysics Data System

1995ApJ...441...28H

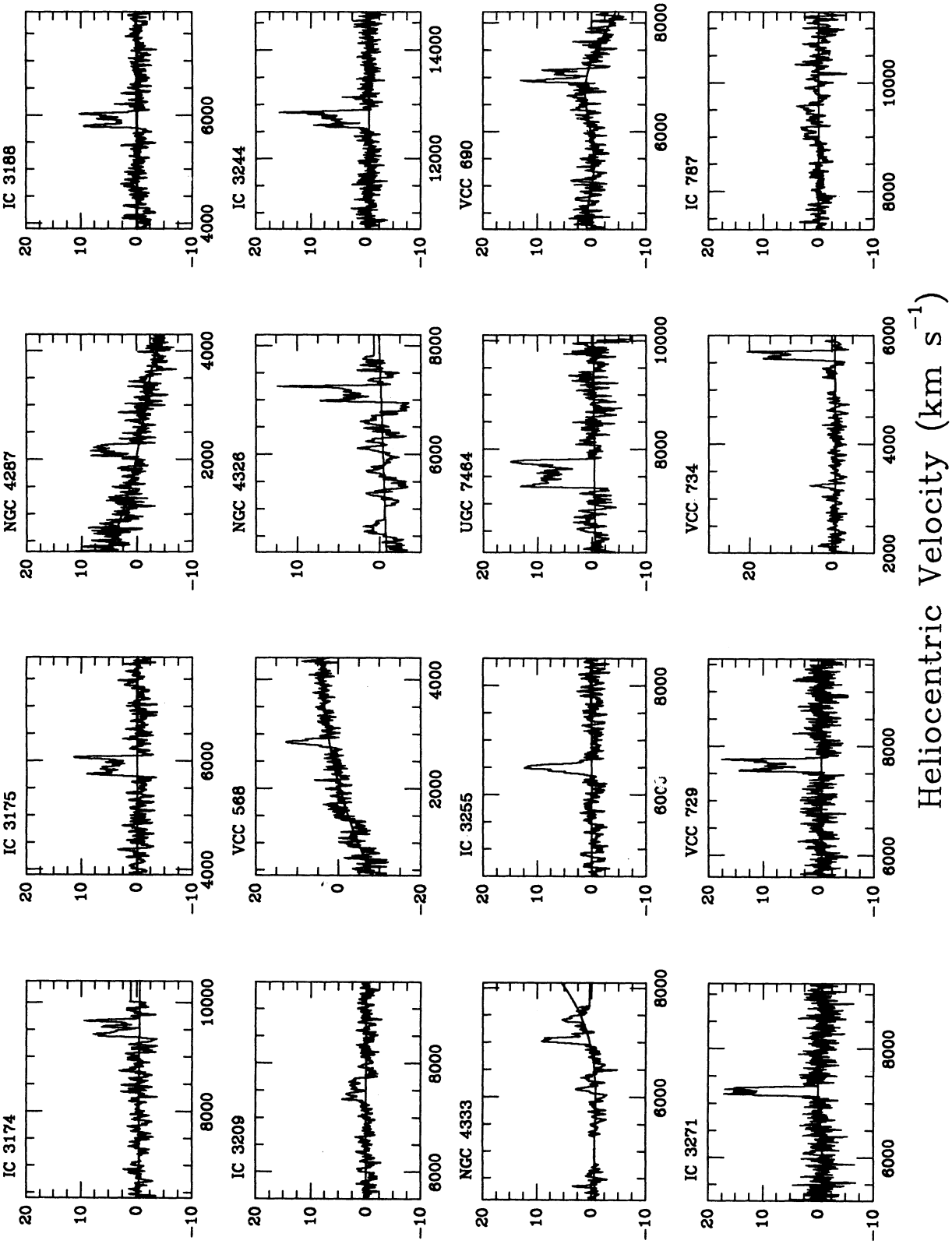

FIG. 1—*Continued*

© American Astronomical Society • Provided by the NASA Astrophysics Data System

1995ApJ...441...28H

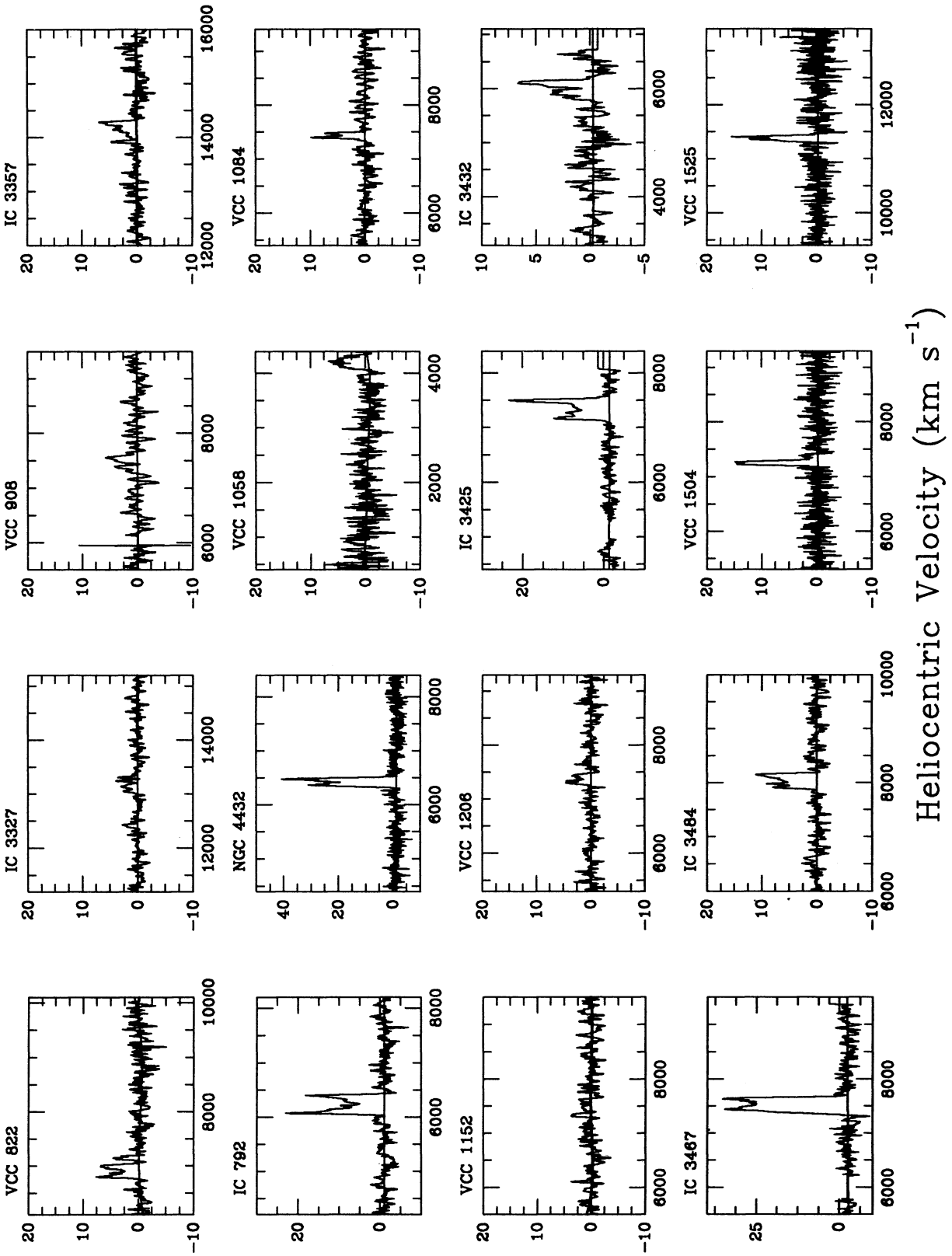

FIG. 1—*Continued*

© American Astronomical Society • Provided by the NASA Astrophysics Data System

1995ApJ...441...28H

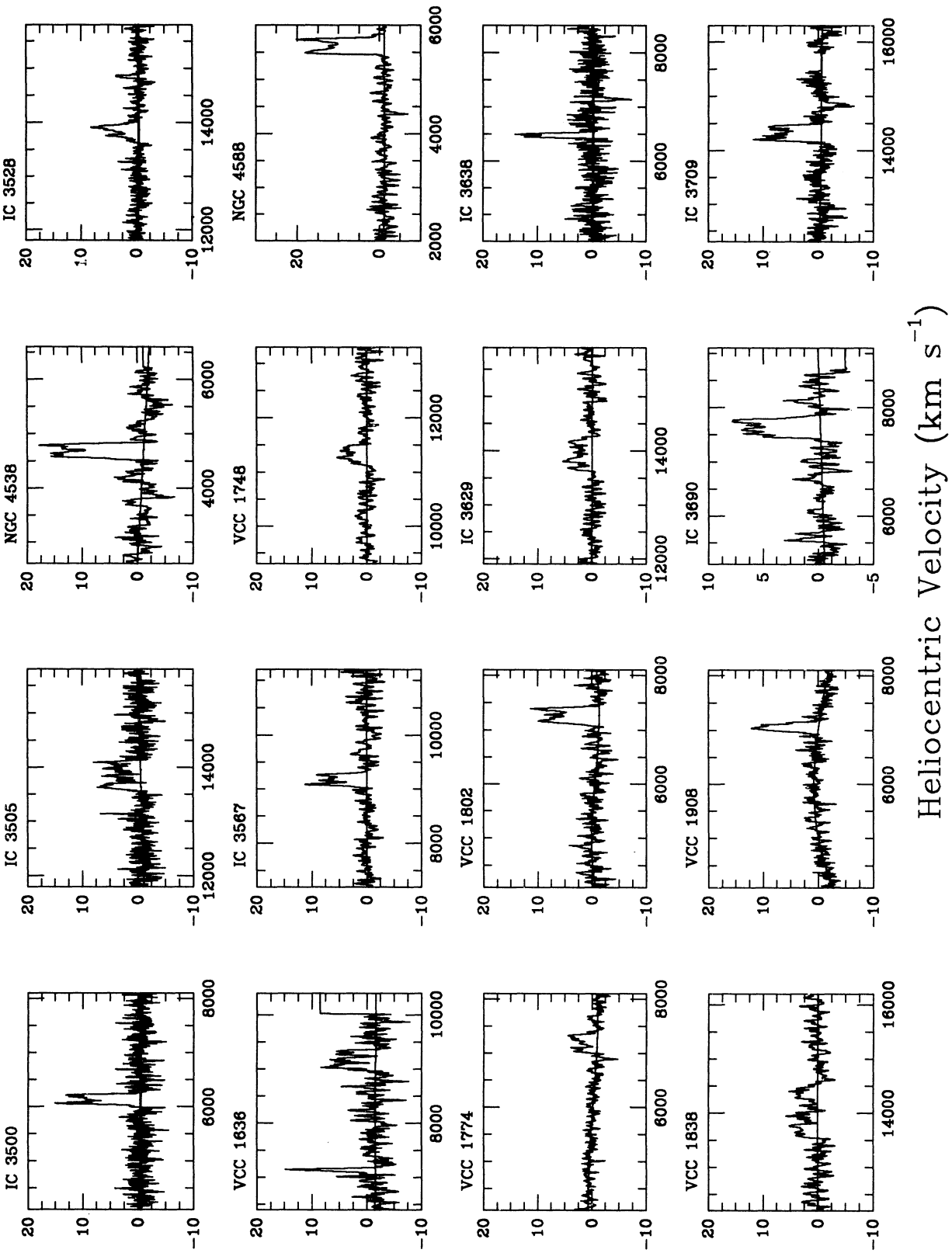

FIG. 1—*Continued*

© American Astronomical Society • Provided by the NASA Astrophysics Data System

1995ApJ...441...28H

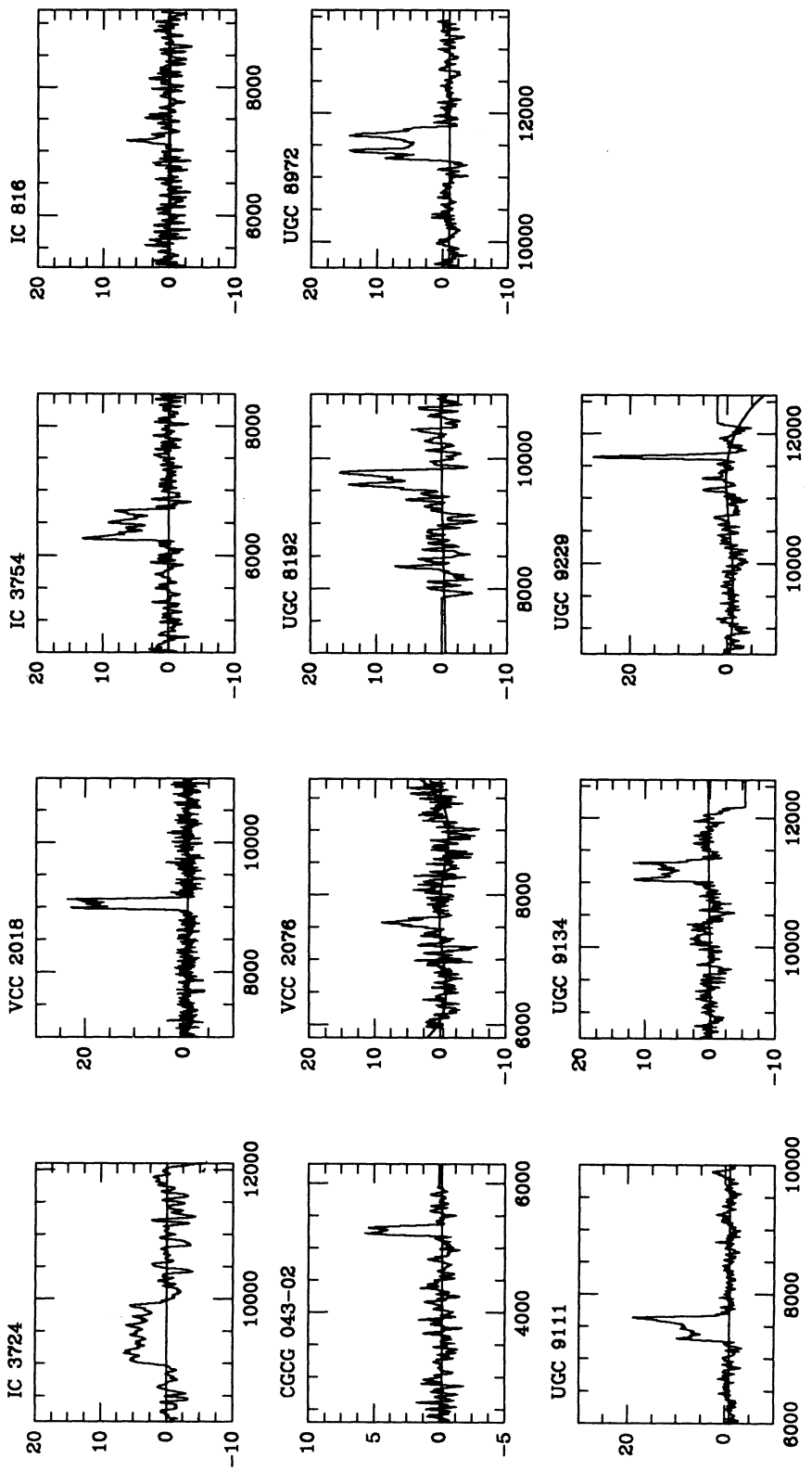

FIG. 1—*Continued*

© American Astronomical Society • Provided by the NASA Astrophysics Data System

1995ApJ...441...28H

UGC 7196.—Higher signal to noise ratio than in Hoffman et al. (1989b, hereafter HLHSW); these new measurements supercede those previously reported.

VCC 40.—Measurements assume that the outer peaks are the two horns of a normal profile. If instead one chooses the two leftmost horns, with the higher velocity spike taken to be from an uncataloged satellite, the results would change to $v_\odot = 6859$ km s^{-1}, $\Delta V_{50} = 221$ km s^{-1}, and $\int S\,dV = 0.93$ Jy km s^{-1}.

UGC 7210.—Detailed comparison with the spectrum we published in HLHSW reveals that the spectrum shown here has the high-velocity edge clearly defined but the low-velocity edge is uncertain, while the previously published spectrum has the low velocity edge well defined but the high-velocity edge is uncertain. If we accept the better defined edge only in each case, the measurements would be $v_\odot = 7094$ km s^{-1} and $\Delta V_{50} = 457$ km s^{-1}.

IC 3039.—Signal-to-noise ratio greatly exceeds that in the spectrum reported in HLHSW. These data supercede HLHSW.

UGC 7230.—No evidence in the H I spectrum of the interaction implied by the morphological type coding in BST. Our velocity and flux are consistent with those reported by Bushouse (1987), who observed UGC 7230 with the 91 m NRAO telescope, but his profile width was much broader than the one we show. Since Bushouse did not publish the spectrum itself, we cannot say whether his broad spectrum results from noise, baseline irregularities, or from more extended emission than that picked up by the narrower Arecibo beam.

NGC 4186.—This object was called NGC 4192b in BST; other names are VCC 101 and UGC 7240. It should not be confused with the galaxy labeled NGC 4186 in Hoffman et al. (1987) and Haynes & Giovanelli (1986, hereafter HG), which was VCC 81. For NGC 4186 = VCC 101 = HGC 7240, HG report measurements consistent with ours.

IC 3060.—Very asymmetric profile. The observed point is about 2′ from the optical center, so it is conceivable that the asymmetry is due to our receiving more flux from one side of the major axis than from the other. If so, the uncertainties in $V_\odot$ and ΔV should be increased, and the flux we report should be regarded as a lower limit.

IC 3107.—Our data are consistent with those previously reported by HG.

UGC 7336.—We differ by more than 1000 km s^{-1} from the velocity reported by WK, whose published spectrum does not quite reach the velocity of our feature. There is no feature in our spectrum at the WK velocity.

IC 3127.—Extraordinarily broad profile for a face-on galaxy.

VCC 331.—Weak feature confirmed by two independent scans.

UGC 7383.—Our data are fully consistent with those reported by HG.

IC 3175 and 3209.—Our data are fully consistent with those reported by HLHSW.

IC 3271.—Consistent with the data reported by HG and with the optical redshift. WK obtained a velocity nearly 4000 km s^{-1} lower and a much broader profile. We are not aware of any source near enough on the sky to crowd into the same beam, and so we are baffled by the discrepancy.

VCC 729.—Fully consistent with data reported by HG.

VCC 822 and 822a.—Although BST make no mention of any irregularity in the optical image nor of any companion within an Arecibo beamwidth, our best interpretation of this spectrum is that it comes from two galaxies: a spiral which produces the normal two-horned profile and a dwarf satellite which produces the narrow spike at slightly higher velocity. CGCG does list a faint galaxy offset by about 4′.

IC 3327, VCC 908, and VCC 1152.—Marginal detections. The profile width and center velocity depend sensitively on what is taken for the edge of the profile on each side, so the parameters are all much more uncertain than the formal uncertainties imply.

IC 3357.—The reported measurements and uncertainties assume that the narrow spike at 14,000 km s^{-1} is the edge of the spectrum. Since that identification is uncertain, the true uncertainties in velocity and width are much larger than the reported formal uncertainties.

IC 792.—Fully consistent with data reported by HG.

VCC 1058.—Profile falls in the region of overlap between the two different velocity range subcorrelators in search mode. Fortunately both edges of the profile are evident in both subcorrelators. Only the lower velocity range is shown, but the data reported are averaged over both velocity range detections.

IC 3432.—Previously measured by Sulentic & Arp (1983) with comparable signal to noise ratio. They obtained $v_\odot = 6037$ km s^{-1}, $\Delta V_{20} = 240$ km s^{-1}, and a flux of 1.1 Jy km s^{-1}. Higher signal to noise ratio would be required to resolve the discrepancy.

VCC 1636.—The spike near 7100 km s^{-1} is due to interface; it does not affect the measurements of the profile.

IC 3690.—Systemic velocity and profile width are consistent with those reported by HG. Our flux is 50% larger than HG's.

IC 3754.—Fully consistent with data reported by HLHSW. The spectrum obtained by WK has much lower signal-to-noise ratio.

VCC 2076.—These data supercede those reported by HLHSW, which had poorer signal-to-noise ratio and the profile at the edge of the spectrum.

UGC 8192.—Consistent with data reported by Freudling, Haynes, & Giovanelli (1988, hereafter FHG).

UGC 8972.—Contact binary with UGC 8973. Spectrum is apparently a fusion of the two; our measurements are for the outermost horns of the four that comprise the spectrum. Not part of the Virgo Cluster background sample.

UGC 9111 and 9229.—Not part of the Virgo Cluster background sample.

UGC 9134.—Not part of the Virgo Cluster background sample. Velocity and profile width are consistent with those reported by FHG, but we record half the flux reported by those authors. Our spectrum is not as symmetric as FHG's, so perhaps the discrepancy is due to pointing errors.

The eight galaxies for which we sought, but did not find, detectable H I, are VCC 256, VCC 359 = IC 3153, VCC 831, VCC 1080, VCC 1134, VCC1347, VCC1793, and VCC 1810. In all cases we searched the velocity range 0–8000 km s^{-1} and achieved an rms noise figure of about 1 mJy. Most likely these galaxies have higher redshifts.

3. GROUP ASSIGNMENTS

The region immediately behind the Virgo Cluster contains two well-known groups: the W group (de Vaucouleurs & Corwin 1986), which figured prominently in our discussion of the Virgo BCD galaxies (Hoffman et al. 1989a), and the M group (Ftaclas, Fanelli, & Struble 1984). Those group assignments were made primarily on the basis of the bright members,

© American Astronomical Society • Provided by the NASA Astrophysics Data System

1995ApJ...441...28H

however, and it is of interest to know whether the groups continue to appear to be isolated and independent associations when fainter galaxies are included. To study this question, we combined the present sample of galaxies in the Virgo background with the corresponding sample from the regions just east and west of the VCC survey area from Lu et al. (1993), along with all galaxies in our previous Virgo papers (HS et al.) and HG, in BPT, in Huchtmeier & Richter (1989), in Bottinelli et al. (1990), or in RC3 that fall in the same regions of the sky with known redshift. We have added some additional galaxies with newly published redshifts from Garcia et al. (1993) and Schombert et al. (1992); these are detailed in Table 2. The combined samples give us a reasonably complete set of galaxies with redshifts to about the magnitude limit of CGCG in the window $10^h < \text{R.A.} < 14^h$, $-2° < \text{decl.} < 20°$, for redshifts in the range $1500 \leq v_\odot \leq 8000$ km s^{-1}. To this set we have applied a "friends of friends" algorithm (Geller & Huchra 1983, hereafter GH; Nolthenius & White 1987) to identify large-scale structures without biasing the results toward spherical objects. The entire redshift range was included in the analysis, although (except for the immediate background of the southern extension of Virgo; see below) we shall consider further only those structures which have mean redshifts in the narrower range 2500–5600 km s^{-1}. The extreme velocities are used only to separate out galaxies which are outliers of structures that fall mainly outside our range of interest. In addition, we excluded galaxies within 5° of M87 with $v_\odot \leq 2500$ km s^{-1} from the analysis (since those galaxies would all be linked into the Virgo main cluster in any case). Our analysis therefore cannot identify the M group (Ftaclas et al. 1984; BPT); to separate it from the rest of Virgo, we would need to use precise distances rather than velocities in our link criterion.

We define relative coordinates between two galaxies by

$$x_{ij} = 2\left(\frac{v_i + v_j}{2}\right) \sin\frac{\theta}{2}$$

and

$$y_{ij} = \chi(v_j - v_i) \cos\frac{\theta}{2},$$

where v_i and v_j are the velocities of the two galaxies and χ is a scale factor to account for galaxies in a bound group having velocity dispersions larger than the velocity differences that would result from Hubble flow alone. Galaxies are said to be "friends" if

$$\sqrt{x_{ij}^2 + y_{ij}^2} < d_L,$$

where d_L is the chosen link parameter. Since our data apply only to a relatively restricted redshift range, we have not adjusted the link criterion to account for the trend toward larger mean galaxy size as distance increases. We found that $\chi = 0.5$, $d_L = 250$ km s^{-1}, strikes an appropriate balance between dividing most of the galaxies among relatively few groups while avoiding percolation across the entire region; $d_L = 75$ km s^{-1} reproduces, by and large, the groups in the catalog of GH. For our purposes it is irrelevant whether the linked entities are genuinely bound groups or not; we seek primarily associations of galaxies that can be taken to lie at a common distance. To emphasize this distribution, we will refer to the associations at $d_L = 250$ km s^{-1} as "clouds" rather than groups. Although some of these clouds are likely to contain a bound subunit, most are not likely to be bound and virialized as a whole. The groups found at the smaller link criterion will be called "subclouds," and many of these are likely to be bound as discussed by GH.

The region immediately behind the southern extension of Virgo, including the much-studied W group, does not separate from the bulk of the Virgo Cluster at the larger link criterion, and so we present only subclouds for this region. Table 3 presents the results of this analysis, with the individual galaxies listed by cloud and subcloud. Column (1) lists identifications of the clouds (numbers offset to the left) and subclouds (e.g., 1A) with applicable GH group numbers in parentheses. The mean right ascension and declination (1950) of the cloud or subcloud are given in colums (2) and (3) in hhmm and ddmm format, respectively. Columns (4) and (5) give the corresponding mean heliocentric velocity and dispersion, both in km s^{-1}. The angular radius $\theta_{1/2}$, in degrees, of a circle containing half the cloud or subcloud members is given in column (6), and θ_{max} in column (7) is the corresponding angular radius, also in degrees, of a circle containing all the members. The number of galaxies in the cloud or subcloud is given in column (8). The members themselves are listed in columns (9)–(12). For those that have an entry in RC3 or VCC, we give only an abbreviated name. Other galaxies, for which we obtained precise positions and redshifts in Lu et al. (1993), have R.A. (hhmmss.s), decl. (ddmmss), and heliocentric velocity (km s^{-1}) given in columns (10), (11), and (12) following the name in column (9).

We have nine clouds in all, ranging up to 56 in membership (an association must have at least four members to be considered a "cloud" in our analysis). The Virgo subcloud VirB which contains the W group, however, has 89 members. These structures are shown on the plane of the sky, in two ranges of redshift and (separately) in the vicinity of the Virgo southern extension, in Figure 2, and all clouds except the southern extension are shown in a wedge diagram in Figure 3. For comparison with the well-studied Coma-A1367 portion of the Great Wall (Ramella et al. 1992; Salzer et al. 1990) which lies

TABLE 2

NEW REDSHIFTS FROM THE LITERATURE

Name (1)	RA (2)	Dec. (3)	Type (4)	B_T (5)	$V_\odot$ (6)	Source (7)
CGCG 014-010	121746.8	3842	Sm		902	GBGGP
MCG 0-32-16	122830.0	15706	Irr		1105	GBGGP
F574-11	123550.4	194924	Sdm	16.4	1363	SBSM
F574-10	124801.8	174424	Sdm		863	SBSM

[a] GBGGP = Garcia et al. 1993; SBSM = Schombert et al. 1992.

© American Astronomical Society • Provided by the NASA Astrophysics Data System

1995ApJ...441...28H

TABLE 3

CLOUDS BETWEEN VIRGO AND THE GREAT WALL

Cloud (1)	$\bar{RA}$ (2)	$\bar{Dec}$ (3)	$\bar{v}_{\odot}$ (4)	σ (5)	$\theta_{1/2}$ (6)	θ_{max} (7)	N_{gal} (8)	Members (9)	(10)	(11)	(12)
1	1031	1414	3032	271	4.3	8.8	31				
1A (GH53)	1005	1303	2814	20	0.9	1.2	4	N3107	U5454	I591	N3153
1B (GH62)	1033	1335	2962	66	0.7	1.5	8	U5695	U5785	N3300	U5781
								U5739	U5760	N3306	
								Z065-072	103444.4	122500	2857
1C (GH63)	1046	1407	3053	61	0.7	0.8	6	P32107	N3391	N3419	U5965
								N3367			
								FS 10	104242.0	135848	3073
rest								U5409	M3-26-43	A1027+16	U6062
								U5436	U5595	U5897	U6104
								U5514	A1020+18	N3433	U6157
								F638-3	102950.4	145424	3160
2	1018	0708	3684	88	0.5	2.3	4	U5537	I601	I602	U5687
3	1041	0001	5596	62	1.2	2.4	7				
3A	1037	−0005	5601	56	0.2	0.6	4	I632	N3325	I633	N3340
rest								U5823	I653	U6011	
4	1139	1552	3517	433	2.6	9.9	56				
4A (GH88)	1139	1728	3333	113	1.1	2.0	24	N3764	M3-30-38	N3802	N3827
								N3768	U6631	N3806	U6687
								N3790	N3800	U6653	N3853
								N3799	N3801	U6666	U6794
								Z097-017	113231.8	180324	3450
								U6569	113315.6	174241	3353
								A1135+1721	113549.2	172141	3447
								Z097-045	113720.4	171354	3209
								Z097-108	114148.0	173518	3345
								Z097-116	114212.0	180841	3441
								U6741	114319.8	172811	3324
								Z097-150	114439.6	165030	3360
rest								U5999	N3731	M2-30-35	N4014
								U6185	U6586	U6747	N4048
								N3559	U6588	U6758	U7032
								I677	U6627	M2-30-37	U7073
								U6424	U6717	I736	U7074
								I2822	N3876	I737	U7100
								U6483	N3869	N3933	
								U6486	N3872	N3934	
								A1109+08	110940.8	85354	3309
								Z096-030	111813.2	193848	4084
								U6362	111818.0	195424	4278
								F571-8	113118.0	193748	3761
5	1118	0242	2529	136	1.8	3.4	4	U6317	N3633	U6402	
								U6379	111912.0	24141	2583
VirA	1209	1840	2362	88	0.8	1.9	6	U7133	N4158	M3-31-64	
								U7170	U7186	U7237	
VirB (W)	1221	0455	2052	362	2.0	9.4	89	V52	V329	V423	U7579
								N4180	V331	N4287	U7612
								N4191	V340	N4289	U7642
								V114	N4260	N4292	N4480
								N4197	N4259	V467	N4496a
								V144	I3148	V468	N4517A
								Z069-108	V344	V479	I3474

© American Astronomical Society • Provided by the NASA Astrophysics Data System

1995ApJ...441...28H

TABLE 3—*Continued*

Cloud (1)	$\bar{RA}$ (2)	$\bar{Dec}$ (3)	$v_{\odot}$ (4)	σ (5)	$\theta_{1/2}$ (6)	θ_{max} (7)	N_{gal} (8)	Members (9)	(10)	(11)	(12)
								N4215	N4261	N4300	V1459
								V172	V351	N4303	N4527
								N4224	N4264	V513	V1550
								V207	I3155	I3225	N4533
								N4233	V367	I3229	N4536
								N4234	N4268	N4324	V1572
								N4235	N4269	V693	N4581
								V223	N4270	V737	N4599
								N4241	N4273	V741	N4632
								V260	N4277	N4378	U7913
								V286	V390	V806	N4666
								V297	N4276	U7512	N4668
								I3131	U7387	V848	N4684
								N4255	N4281	N4412	
								V320	V415	N4420	
								U7354	U7394	V985	
VirC	1222	0043	2168	67	1.2	2.1	7	U7370	DDO 121	N4418	U7625
								U7396	N4385	M0-32-13	
VirD	1233	0656	2019	70	0.7	1.6	4	N4532	DDO 137	I3617	
								anon	123037.5	60924	1919
VirE	1237	0726	1771	113	0.8	2.2	7	N4570	U7802	N4612	I3716
								I3589	V1789	N4623	
VirF	1253	0818	2675	102	0.1	0.2	5	N4791	U8042	U8045	N4803
								N4795			
VirG	1257	1409	1986	59	0.5	0.8	4	U8085	M2-33-43	N4866	U8114
6	1225	0552	4623	583	3.0	7.6	36				
6A	1216	0856	4370	77	0.3	0.4	4	V248	P39502	I3134	V406
rest								I3040	N4296	U7607	V1583
								V116	V550	Z042-136	N4576
								V198	N4334	U7644	U7806
								N4246	V734	V1322	V1864
								N4247	U7516	V1362	U7873
								V277	V858	N4496b	
								I3136	V899	V1456	
								Z042-027	V1058	N4538	
								A1244+03	124454.9	31840	5268
								Z043-029	124527.0	44217	4889
								Z043-085	125548.6	50923	4877
7	1310	−0035	5559	140	1.7	2.6	12	I849	N4996	U8340	N5104
								I850	N4999	I4218	
								U8223	U8265	U8360	
								A1303-01	130347.0	−12440	5558
								A1316-02	131630.0	−21500	5480
8	1331	−0028	3822	425	1.3	2.6	12	M0-34-35	N5183	U8526	I903
								U8473	N5184	N5211	Z017-048
								U8474	U8521	Z017-031	Z017-054
9 (GH127+130)	1355	0605	4531	333	2.2	8.2	19	N5327	U8816	N5386	Z074-035
								I947	U8861	N5387	N5414
								U8787	N5374	U8896	N5418
								N5335	N5384	U8906	
								U8796	N5382	U8918	
								F721-V3	135804.2	91405	4148

© American Astronomical Society • Provided by the NASA Astrophysics Data System

1995ApJ...441...28H

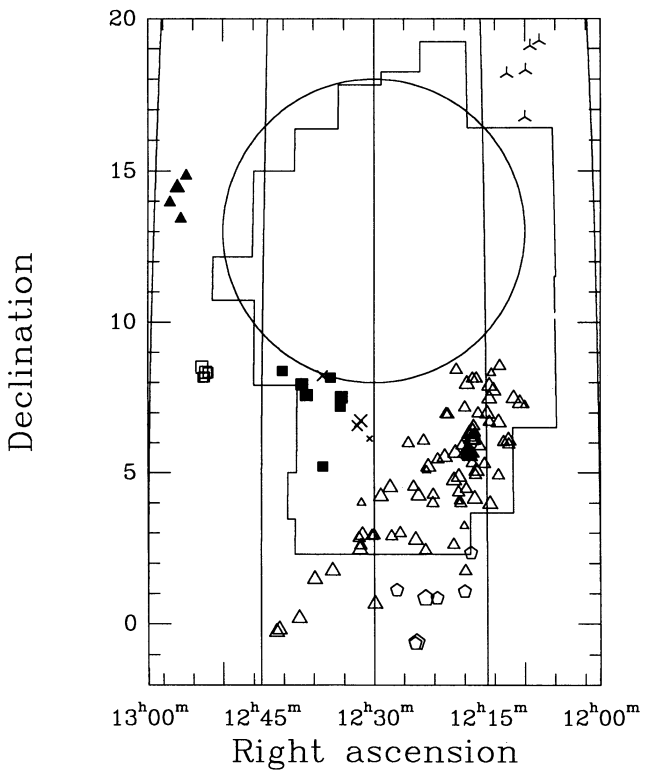

FIG. 2*a*

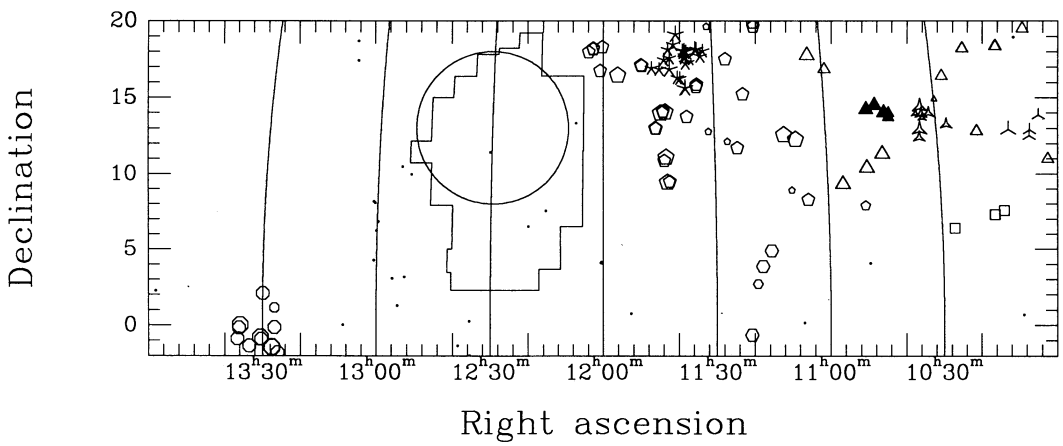

FIG. 2*b*

FIG. 2.—Identified clouds of galaxies (*a*) in the immediate background of Virgo, (*b*) in the redshift range 2500–4000 km s^{-1}, and (*c*) 4000–5600 km s^{-1}. The members of each cloud and each subcloud as defined in Table 3 are shown with dots of a different style: in (*a*), the VirA subcloud is shown with three-pointed asterisks, VirB (which includes the W group) with open triangles, VirC with open pentagons, VirD with exes, VirE with filled squares, VirF with open squares, and VirG with filled triangles. In (*b*), Cloud 1 is shown with three-pointed symbols: asterisks for subcloud 1A (GH 53), stars for 1B (GH 62), filled triangles for 1C (GH 63), and open triangles for members of the cloud that are not also members of a subcloud; Cloud 2 is shown with open squares; Cloud 4 is shown with open pentagons, with 4A (GH 88) indicated by five-pointed asterisks; Cloud 5 by open hexagons; and Cloud 8 by open octagons. In (*c*), the open hexagons go to Cloud 3, while 3A gets six-pointed asterisks; squares to Cloud 6, while 6A gets Xs; pentagons to Cloud 7; and triangles to Cloud 9 (GH 127 and GH 130). Unaffiliated galaxies in each redshift range except (*a*) are represented by small dots. In each panel, the VCC survey boundary and a 5° circle representing the core fo the Virgo Cluster are shown. Panel (*d*) shows the galaxies beyond 5600 km s^{-1} in our survey area, with different symbols for different velocity ranges: triangles for 5600–9000 km s^{-1}, squares for 9000–12,000, and pentagons for 12,000–20,000 km s^{-1}.

just north of our sample, we include the more distant ($v_\odot \geq$ 5600 km s^{-1}) galaxies from our sample in Figures 2*d* and 3*b*.

Notes on particular cases follow.

Cloud 1 is quite stable over a wide range of scale factor and link criteria and is confirmed by a dendogrammatic analysis along the lines of Tully (1987). It incorporates three of GH's groups, which might individually be bound, but the structure as a whole is probably not bound (and certainly not virialized). If the link criterion is increased, this cloud merges with cloud 4 to the east.

Cloud 2 is a small quartet of galaxies that is quite stable against changes in scale factor and link criteria and appears in the dendogrammatic analysis. Its members are mostly too faint for it to appear in group assignments based on the CfA redshift

© American Astronomical Society • Provided by the NASA Astrophysics Data System

1995ApJ...441...28H

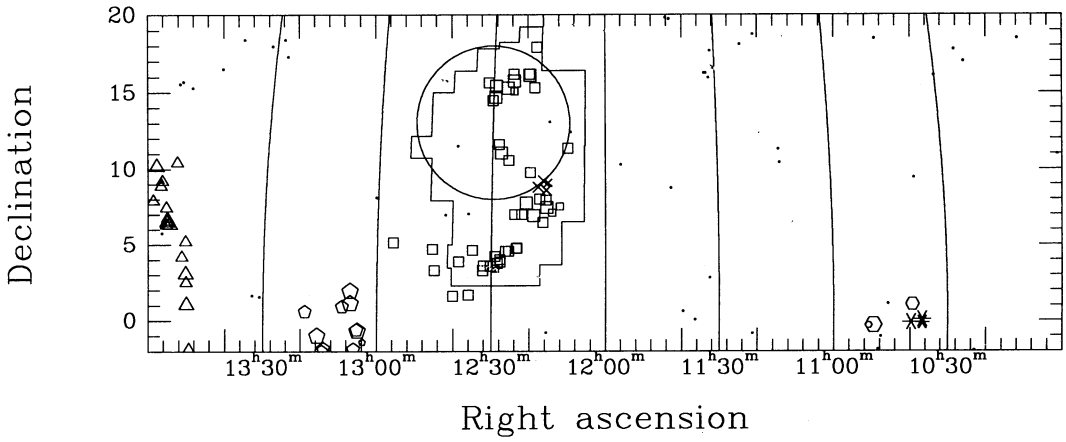

FIG. 2c

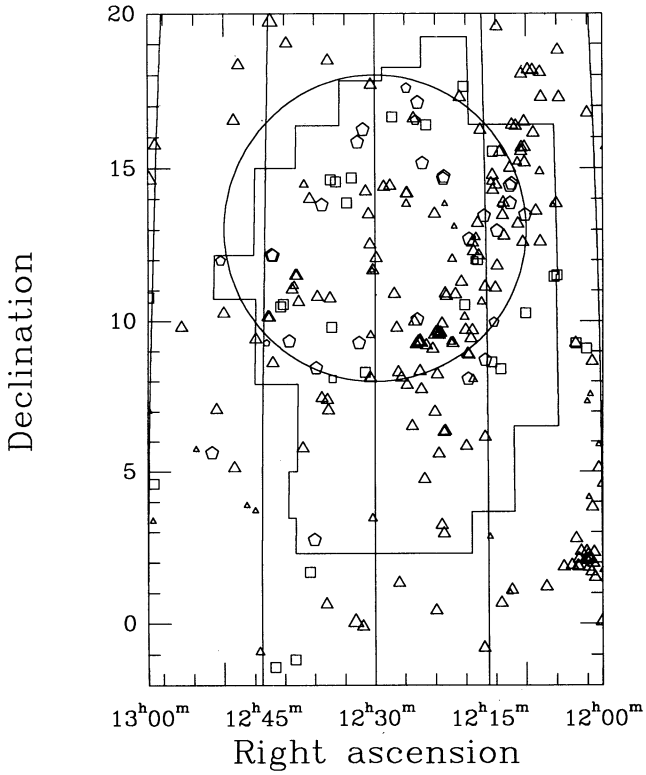

FIG. 2d

survey (Huchra et al. 1983). It is not clear whether the group is bound or not.

Cloud 3 remains distinct from larger clouds within the Great Wall unless the link criterion is increased substantially. Subcloud 3A has members that are mainly too faint for the group to have been identified by GH.

The core of Cloud 4 is the large group GH 88 identified by us as subcloud 4A, and the much smaller group GH 96 is contained as well although it does not show up in our $d_L = 75$ km s^{-1} analysis. Our scanning of the Palomar Sky Survey plate, using the Minesota Automated Plate Scanner (hereafter called MAPS: Humphries, Pennington, & Ghigo 1987; Dickey et al. 1987; Odewahn et al. 1992), identified a great many fainter members of the cloud. The core (GH 88) most likely is bound and virialized; the extended cloud almost certainly is not. A larger link criterion causes this cloud to merge with Cloud 1; however, in the dendogrammatic analysis it merges instead with structure behind the Virgo Cluster core.

Cloud 5 is a diffuse quartet near our southern boundary. It may merge with larger structure further south.

The well-known W group which is thought to lie about 1.7 times farther away from the Local Group than the core of the Virgo Cluster (Hoffman et al. 1989a and references therein) does not show up in our analysis at $d_L = 250$ km s^{-1}. To fully resolve it from the core and southern extension of the Virgo Cluster would require the use of accurately measured distances rather than velocities for the third dimension (Fukugita et al. 1993). A more diffuse cloud to the east of the southern extension, at redshifts similar to the W cloud, similarly cannot be distinguished from the southern extension at the larger link criterion. At $d_L = 75$ km s^{-1}, however, we pick out (as VirB) a portion of the southern extension which has the W group as its core. The membership of VirB, as defined here, agrees surprisingly well with that defined by BPT using morphology and other distance indicators to supplement the redshift information in deciding group membership. Several other, smaller, subclouds are picked out as well in our analysis, as shown in Figure 2*a*. Most of these structures are probably falling toward the Virgo Cluster from behind (Tully & Shaya 1984).

Cloud 6 is almost superposed on the W cloud on the plane of the sky but at significantly higher redshift. Only a few of its members are bright enough to have appeared in GH. When the W cloud and Cloud 6 (along with a group at a redshift of 5979 km s^{-1}) are shown on the same map of the sky, they give the appearance of a well-defined filament stretching across the southern extension of the Virgo Cluster. However, they are sufficiently distinct in redshift that neither the percolation analysis presented here nor the dendogrammatic analysis causes them to merge; instead, percolation occurs east to west across the sample at smaller link criterion than required for percolation north to south, or along the "filament." We conclude that the apparent filamentary structure is only a projection effect.

Cloud 7 is sufficiently distinct in redshift from the Great Wall that it does not merge with other Great Wall groups unless the link is increased substantially. However, it may link to structures further south. Cloud 8 also lies near our southern boundary (at smaller redshift) and may link to lower redshift

© American Astronomical Society • Provided by the NASA Astrophysics Data System

1995ApJ...441...28H

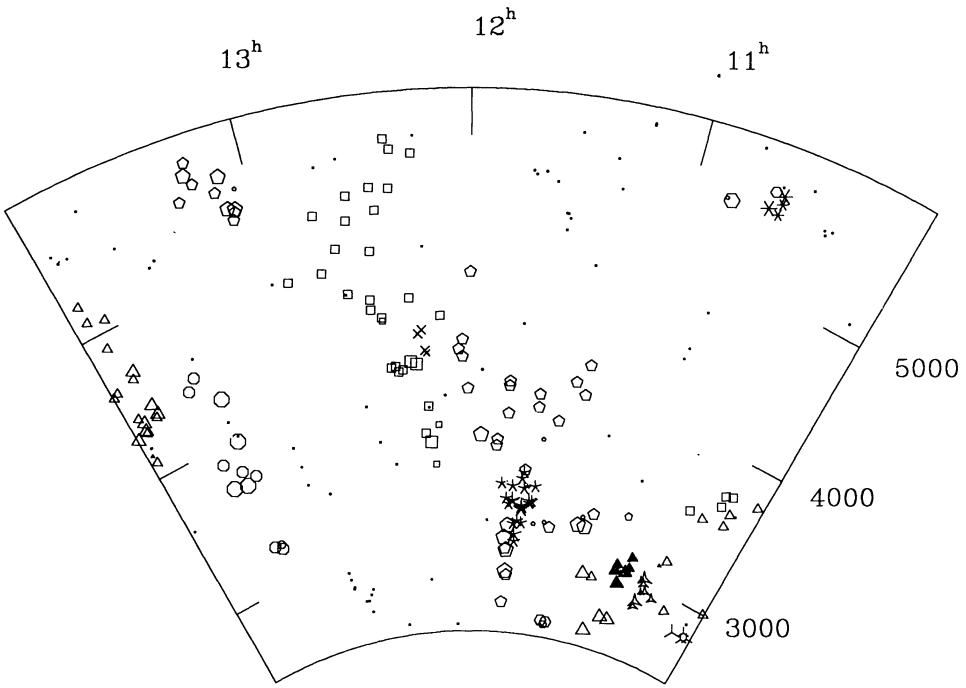

FIG. 3a

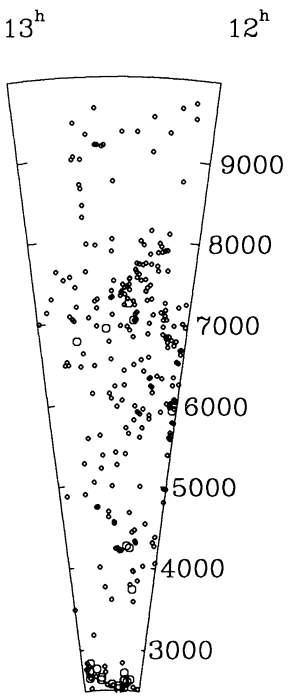

FIG. 3b

FIG. 3.—(*a*) A wedge diagram representation of the clouds illustrated in Fig. 2. The same symbols as in Figs. 2*b* and 2*c* are used for each cloud. The radial coordinate is heliocentric velocity, and the polar coordinate is right ascension. (*b*) A wedge diagram from the more distant galaxies in the survey area shown in Fig. 2*d*. Coordinates are the same as for panel (*a*). The size of each circle indicates the apparent magnitude of the galaxy, with the largest circles representing the brightest galaxies.

structures further south. Both clouds are stable against changes in the link criterion and appear in dendogrammatic analyses also.

Cloud 9 lies near the eastern edge of the volume studied and may link to structures further east. If the link is made slightly smaller, the chain breaks into two pieces. Groups GH 127 and GH 130 are incorporated into these two pieces; however, neither is sufficiently compact so as to be identified as a separate entity by our smaller link criterion.

Acquisition of *I*-band CCD photometry for the members of these clouds, for a cloud-by-cloud Tully-Fisher analysis, is underway and will be reported separately. Preliminary results, restricted to the bright galaxies in the sample, are given in Lu, Salpeter, & Hoffman (1994). It is intriguing that percolation proceeds east to west, perpendicular to the supergalactic plane, for this sample; it will be interesting to see whether this result holds when the sample is extended to a larger area on the sky.

Figure 3*b* may be compared to similar wedge diagrams in Salzer et al. (1990) showing the Great Wall just north of the VCC survey region. The Great Wall is not so clearly delineated in our plot, but we would need a deep sample covering a larger area of the sky to say whether we are seeing a locally more diffuse section or the southern edge of the Great Wall. The rather vague structure running across Figure 3*a* from R.A. $\sim 11^h30^m$ to $\sim 13^h30^m$, at redshifts from ~ 3500 to 5000 km s^{-1}, matches up quite well with a similar structure just to the north, clearly visible in Figure 3 of Salzer et al. (1990). This structure appears to form the front wall of the Coma void.

4. VOIDS AND THE LUMINOSITY FUNCTION IN REGIONS OF HIGH AND LOW DENSITY

Some theoretical considerations (Salpeter 1993; Babul & Rees 1992; Lacey & Silk 1991; Tyson & Scalo 1988; Dekel & Silk 1986) have led to the speculation that the luminosity function for galaxies in low-density regions (e.g., voids) may be skewed toward dwarf galaxies vis-à-vis that for high-density regions (e.g., superclusters). Attempts to ascertain whether or not this is true observationally have obtained conflicting results to date (Eder et al. 1989; de Lapparent, Geller, & Huchra 1989; Binggeli, Tarenghi, & Sandage 1990; Briggs 1990; Salzer et al. 1990; Weinberg et al. 1991; Hoffman, Lu, & Salpeter 1992; Iovino et al. 1993). We approach the subject for the region between Virgo and the Great Wall by subdividing the volume into "honeycomb" cells in (R.A., decl., redshift) space, computing the density (corrected for the missing faint end of the luminosity function) in each cell, then computing luminosity functions separately for high- and low-density cells.

Our bins are $4^\circ \times 4^\circ \times 1000$ km s^{-1} in size, and we average together eight nearest neighbors for those bins with $cz < 3500$ km s^{-1} so that the regions within which we compute densities do not differ in volume by more than a factor of 4. We are particularly interested in galaxies likely to be H I–rich, and so we count only galaxies of morphological type Sa through Im, and adopt (solely for the purpose of correcting the number counts for the missing faint end of the luminosity function) the luminosity function obtained by Binggeli, Sandage, & Tammann (1988) for spirals and irregular galaxies in the Virgo Cluster for which the data is most nearly complete. A reasonable analytic fit to their data is given by

$$\phi(M) \propto \exp\left(-\left|\frac{M+18.5}{2.1}\right|^3\right) + \exp\left(-\left|\frac{M+15.5}{1.6}\right|^3\right), \quad (1)$$

where M is the absolute magnitude in the B_T system. The first term is a fit to the spiral LF alone, and the second fit the LF for irregulars alone; fortuitously, they have very nearly the same

© American Astronomical Society • Provided by the NASA Astrophysics Data System

1995ApJ...441...28H

normalization. We take the magnitude limit to be $B_T \leq 15.5$ for our sample since we appear to be reasonably complete to about the limit of CGCG in and around the VCC survey area. For each galaxy in the region of interest, we then compute the number of galaxies missing at the same redshift by integrating over the tail of that LF.

The number densities—of late-type galaxies ($T \geq 3$) only—in these honeycomb cells are shown in Table 4. The units for density in Table 4 are 10^{-6} (km s^{-1})^3, and in each cell of the table we display an "H" (for "high" density) if the density exceeds 0.3 in those units; an "M" (medium) for densities in the range 0.1–0.3; an "L" (low) for 0.03–0.1; and the cell is left blank if the density is below 0.03. There is a prominent void behind the northeast quadrant of the Virgo Cluster, extending from 3500 km s^{-1} up to the Great Wall at 5500 km s^{-1}, and the entire volume between 3500 and 5500 km s^{-1} is significantly lower in density than the Local supercluster (even with the cluster core removed) and the portion of the Great Wall beyond 5500 km s^{-1}. To compare luminosity functions in low- and high-density environments we adopt two strategies: (1) divide cells into "high-," "medium-," and "low-" density bins irrespective of their location, and compute LFs for each bin separately; and (2) identify cells in and around the most prominent void, and compute LFs for those and for all remaining cells separately. We employ the "ϕ/Φ" method as described in Binggeli et al. (1988) to determine the luminosity function nonparametrically (the Virgo Cluster fit is used only to categorize the cells by density). Within the scatter due to relatively small numbers of galaxies (170 in total out to 5500 km s^{-1}), we cannot distinguish the resulting luminosity functions from one another nor from the analytic fit to the Virgo Cluster LF. Note, however, that we have no rich cluster cores in our sample, so our results are not necessarily in conflict with those of Iovino et al. (1993) who find differing LFs for high- and low-density regions of the Perseus-Pisces supercluster.

In light of the fact that most spirals of very low surface brightness (SB) (of which Malin I is the prototype) have been found in low-density environments (Bothun et al. 1993; Knezek 1993), it is of interest to inquire whether or not there is a significant difference in mean optical surface brightness (SB),

TABLE 4

NUMBER DENSITIES IN HONEYCOMB CELLS

Dec.	12^h06^m	12^h22^m	12^h38^m	12^h54^m
1500–3500 km s^{-1}				
0–4°	H	H	M	M
4–8°	H	H	M	M
8–12°	H	H	M	M
12–16°	H	M	L	L
16–20°	H	M	L	L
3500–4500 km s^{-1}				
0–4°			L	
4–8°	L	H		
8–12°		M	L	
12–16°	L			
16–20°	M			
4500–5500 km s^{-1}				
0–4°	L	L	M	
4–8°		L	L	
8–12°				
12–16°		L		
16–20°	L			
5500–6500 km s^{-1}				
0–4°	M			
4–8°	M	L	L	
8–12°	L	M	L	L
12–16°	L	L	L	L
16–20°	L	L		L
6500–7500 km s^{-1}				
0–4°	L	L	L	L
4–8°	L	M	L	L
8–12°		H	L	
12–16°	M	L		
16–20°	M			
7500–8500 km s^{-1}				
0–4°		L		
4–8°				L
8–12°		L	L	
12–16°	M	L	L	
16–20°			L	

NOTE.—Density assignments: H, >0.3; M, 0.1–0.3; L, 0.03–0.1; blank, <0.03.

© American Astronomical Society • Provided by the NASA Astrophysics Data System

1995ApJ...441...28H

TABLE 5

REDSHIFT STATISTICS FOR BST GALAXIES

Dec.	B_T mag	Optical cz < 8000	Optical cz > 8000	H I cz < 8000	H I cz > 8000	H I Und. > 8000	No Info
< 8°	14.5–15	2	0	22	0	2	6
	15–15.5	2	0	21	0	5	10
> 8°	14.5–15	31	14	10	0	1	5
	15–15.5	24	16	18	5	0	9

hydrogen mass–to–blue light ratios M_H/L, or H I deficiency parameter, Def $\equiv \log M_H(D_{25}) - \log M_H$(obs) as in Haynes & Giovanelli (1984) and Gavazzi (1987), between high- and low-density regions. We would expect Malin I–type objects to have low SB and large M_H/L compared to normal spirals. Dividing our honeycomb cells (restricted to redshifts $\leq$5500 km s^{-1}) into "high-," "medium-," and "low-" density bins (so chosen that we have comparable total numbers of galaxies in each bin, e.g., 99 galaxies in the "high"-density cells, 65 in "medium," and 42 in "low," the last including cells shown as blanks in Table 4), we find no statistically significant differences among the three regions in M_H/L, Def, or SB. Def has a small positive mean in all three regions (0.06 ± 0.04, 0.11 ± 0.06, and 0.14 ± 0.08 for "high," "medium," and "low" regions, respectively). Since "high" does not contain any clusters of galaxies, it is not surprising that all three regions should have normal H I content. The lack of a difference in "low" regions is most likely due to our selection criteria: We are limited to galaxies that are recognized as late-type systems in visual inspections of POSS or du Pont plates. Very low surface brightness disks (like the giant spiral Malin I and, especially, similar objects with smaller disk radii) are likely to be missing from our sample.

To summarize: We have no direct evidence in our data for any kind of density dependence. However, this does not contradict the subtler environmental effects found in other studies: There is a tendency for low surface brightness (but not necessarily dwarf) galaxies with more extended disks to be found in low density regions (Knezek & Schneider 1993; van Gorkom 1993).

5. DISK GALAXY STATISTICS AND THE LINE OF SIGHT TO 3C 273

The line of sight to the quasar 3C 273 lies just south of the VCC survey boundary, so our analysis of the large-scale structure between Virgo and the Great Wall leaves us in position to assess the likelihood that the low-redshift Lyα absorptions identified by Bahcall et al. (1991) and Morris et al. (1991) are associated with the large-scale structure defined by normal galaxies. The two groups find Lyα absorption lines at cz = 1012, 1582, 2200, 6535, 7860, 8826, 9865 km s^{-1} and higher redshifts (starting at 14,700 km s^{-1}) for which we have little information about galaxy redshifts. Our discussion parallels that of Salzer (1992), but we have more redshift data for the southern extension of the Virgo Cluster (see also van Gorkom et al. 1993). Morris et al. (1993) supply imaging and multifiber spectroscopy for faint galaxies in the area immediately around the line of sight to the quasars; we will put their fine-scale findings into the context of the large surroundings. There are no galaxies in UGC or CGCG (with or without redshift) within 30′ of the QSO line of sight, and prior to the work of Morris et al. (1993) there were no galaxies with known redshifts in the Great Wall range close to the QSO. However, the multifibre spectroscopy has added several closer candidate disk systems, most significantly fainter than the CGCG magnitude limit. We are also able to add one galaxy, MCG 0-32-16, within 34′ of the line of sight. The galaxy is bright enough to be in CGCG (CGCG 014-054) and has an entry in RC3, but it is too faint to have been included in Salzer's (1992) observing list and too bright to have been one of Morris et al.'s (1993) candidates for multifiber spectroscopy. However, it has a recent published velocity (Garcia et al. 1993) close to that of the nearest 3C 273 absorption line and therefore has some effect on the statistics discussed below.

Here we discuss the galaxy number density and fractional area covered by optical disks for regions up to 10° or 20° away from 3C 273. In a companion paper (Salpeter & Hoffman 1995) we discuss the immediate vicinity of the line of sight.

For the observed and cataloged optical galaxies in a given velocity range, we can calculate the average fraction of the sky covered by the optical areas of galaxy disks out to the 25 mag arcsec^{-2} isophote, say. We need to correct this fraction for the faint end of the luminosity function, missed because of an apparent magnitude cutoff. Since the mean optical surface brightness does not depend very strongly on absolute luminosity, we calculate the correction factor for total luminosity of all galaxies in a given volume, using the luminosity function in equation (1). Assuming an apparent magnitude cutoff $B_T \leq$ 15.5 as in the previous section, for our sample in $v_\odot$ < 3500 km s^{-1} our estimate for this correction factor is a mere 1.02; for the data available in $3500 < v_\odot < 9500$ km s^{-1} the factor jumps to $\sim$1.8. For the very small area in the immediate vicinity of the 3C 273 line of sight (see § 5.2, below), the redshifts from Morris et al. (1993) extend about 3.5 mag fainter and the correction factor would again be close to 1.02 and thus unimportant.

Our sample does not quite have complete redshift information, and since the missing redshifts are concentrated at the fainter magnitudes ($14.5 < B_T \leq 15.5$) there is likely to be a greater deficit in more distant redshift bins. We correct for this bias as follows: First, we consider galaxies from BST north of 8° declination separately from those south of 8°. The northern BST galaxies in the 14.5–15.5 mag range have much more complete optical redshift data than the southern set, as detailed in Table 5. In Table 5, "optical" means that the redshift was available in BST, before H I data were obtained.

H I redshift searches at Arecibo typically start in the range 0–8000 km s^{-1}, and it is quite unusual for a late-type galaxy with cz < 8000 km s^{-1} and $B_T \leq$ 15.5 to go undetected in a 5

© American Astronomical Society • Provided by the NASA Astrophysics Data System

1995ApJ...441...28H

minute scan. So we presume that galaxies searched but undetected in H I have redshifts >8000 km s^{-1}. For BST galaxies north of 8° we infer simple multiplicative factors of 60/55 (61/55) for areas assigned to galaxies with $cz < 8000$ (>8000) km s^{-1} and $14.5 < B_T \leq 15.0$, and 72/63 irrespective of redshift for $15.0 < B_T \leq 15.5$. We use the same factors for galaxies at $\delta < 2.^\circ5$ since Salzer (1992) has comparable optical and H I data to a comparable magnitude limit.

For BST galaxies south of 8° and for all galaxies north of 2.°5 but outside the BST area, the corrections are more problematic. Ignoring the few essentially randomly chosen BST galaxies in the 14.5–15.5 mag range with optical redshifts, we can use the breakdown of H I redshifts above and below 8000 km s^{-1} in each half-magnitude bin to estimate how the unobserved galaxies are distributed in redshift. Then the appropriate multiplicative factors for galaxies with known redshift (all having $cz < 8000$) are 29.54/24 for $14.5 < B_T \leq 15.0$ and 31.21/23 for $15.0 < B_T \leq 15.5$, each multiplied by the ratio of the total area (excluding the regions included in the above paragraph) to the BST area south of 8°. We distribute the estimated number of galaxies with $cz > 8000$ uniformly over the range 7500–13,500 km s^{-1}, approximately as the known redshifts >8000 km s^{-1} are distributed in the northern region.

The declination 0°–8° region has 3C 273 somewhat south of its center. In our analysis (§ 3) the W cloud has 2 σ velocity limits 1328–2776 km s^{-1}, and BPT find comparable limits, 1387–2811 km s^{-1}. The velocity distribution is not Gaussian, however, and we (by definition) have no W cloud members below 1500 km s^{-1}, while BPT have only three. The southern extension, according to BPT, ranges (at 2 σ) between 616 and 1408 km s^{-1}, and the W′ cloud which bridges the W cloud to the main Virgo Cluster component B has limits 708–1912 km s^{-1}. We therefore select 1500 km s^{-1} as a reasonable redshift boundary separating galaxies at the distance of Virgo from those significantly further beyond. A redshift of 3500 km s^{-1} is slightly above the highest redshift in the W cloud or any of the other subclouds in the near background of Virgo, and for comparison it is convenient to keep bins of constant 2000 km s^{-1} redshift width.

The statistics are presented in Table 6 as fractions of sky area covered by the optical galaxy disks, i.e., as the ratio of the area within the 25 mag arcsec^{-2} isophote (A_{25}) to the total area on the sky $A_{\rm tot}$. The highest redshift bin in Table 6 has two entries for each region: one, in parentheses, giving the result with no correction for missing redshifts, and a second entry without parentheses which incorporates the corrections discussed above. The first entry should be regarded as a lower limit; the second is our best guess at the true result, with an uncertainty which is a large fraction of the difference.

With the exception of the velocity range 3500–5500 km s^{-1}, the two declination ranges in Table 6 give similar results and we average over them. The main result of Table 6 can then be summarized in terms of two round numbers: For $0 < v_\odot < 3500$ km s^{-1}, the fractional optical area in each 2000 km s^{-1} redshift bin is about 3×10^{-4}, while for $3500 < v_\odot < 10{,}000$ km s^{-1} the corresponding fraction is about 3×10^{-5}. For a uniform spatial distribution of galaxies, these fractions would be proportional to the velocity range covered (as in Olbers's paradox), so the actual galaxy number density is larger for the lower velocity range by a little more than a factor of 10. This lower velocity range traverses the Virgo Supercluster and is thus fairly typical of a "high-density region." Our higher redshift range includes the "almost void" region between Virgo and the Great Wall, but also part of the outskirts of the Great Wall itself (6000–12,000 km s^{-1}; Ramella et al. 1992). Our area on the sky is far enough from the dense parts of the Great Wall, however, that the whole velocity range 3500–10,000 km s^{-1} in Table 6 can be thought of as a "typical, moderately low density region."

TABLE 6

STATISTICS OF DISKS, 11:58 < R.A. < 13:02

$v_\odot$	$\frac{A_{25}}{A} \times 10^6$	
km s^{-1}	0–8°	8–20°
(1)	(2)	(3)
< 1500	285	395
1500–3500	271	316
3500–5500	25.4	5.7
5500–7500	29.8	57.0
7500–9500	(7.4)29.1	(19.9)37.4

There are three Lyα absorption lines observed on the line of sight to 3C 273 in our lower velocity range (<3500 km s^{-1}) compared with our fractional optical area (summed over two 2000 km s^{-1} bins) of 6×10^{-4}. If we postulate that the actual areas responsible for Lyα absorption are simply some factor F times the optical area of ordinary visible galaxies, then $F \approx 5 \times 10^3$, and we require a diameter for each galaxy 70 times larger than the optical. For our higher velocity range (extrapolating to 10,000 km s^{-1} to include the Lyα line at 9865 km s^{-1}) there are four absorption lines compared with a fractional area of 1×10^{-4}, so $F \approx 4 \times 10^4$, and we require a nominal absorption diameter about 200 times larger than optical. This illustrates a result already suggested by Morris et al. (1993): For Lyα absorption lines at low redshifts z, just as for large z, the number of lines per ordinary galaxy is lower in regions of high galaxy density (superclusters) than in average regions. Expressed in an alternative way, the number of lines per unit volume does not depend appreciably on the galaxy density when averaged over larger volumes. However, this need not mean that absorption clouds are completely unclustered and unassociated with galaxies: their clustering on the very large scale (I) may be reduced by biassing effects, but they could reside in clouds (intermediate scale II) which also contain galaxies. In particular, we shall suggest (see the companion paper, following) that the low-density "clouds of galaxies and groups" in the semivoids contain a much larger ratio of invisible absorption clouds to ordinary galaxies than do the denser galaxy groups within the Local Supercluster.

Our description above in terms of a multiplicative factor F has the advantage that it does not depend on the value of the Hubble constant H_0, but we can restate the required disk areas per ordinary galaxy in terms of absolute sizes. For our luminosity function (1), the total number of very faint galaxies converges and (assuming a Virgo distance of 19 Mpc and $H_0 = 75$ km s^{-1} Mpc^{-1} from now on), the average optical area (out to the 25 mag arcsec^{-2} isophote) is 60.4 kpc^2, corresponding to a circular disk of radius 6.2 kpc at a random inclination. The corresponding absolute blue magnitude is about -18. In § 3 of the following paper (Salpeter & Hoffman 1995), we shall associate a length scale $R'_{\rm for}$ with each ordinary galaxy, purely for counting purposes. We define this radius $R'_{\rm for}$ per ordinary galaxy in terms of the factor F as $R'_{\rm for} = F^{1/2} \times 6.2$ kpc, which gives $R'_{\rm for} \simeq 500$ kpc and 1.5 Mpc, respectively, for $v_\odot$ below and above 3500 km s^{-1}.

© American Astronomical Society • Provided by the NASA Astrophysics Data System

1995ApJ...441...28H

6. SUMMARY AND CONCLUSIONS

This paper has presented H I data for most of the "background" galaxies from the BST Virgo Cluster Catalog. With the 80 redshifts presented here added to optical redshifts available in BST, we now have redshift information for 100 of the 137 "background" galaxies. This sample has allowed us to explore the large-scale structure of the volume of space between the Local Supercluster and the Great Wall at $cz \sim 5500$–$13{,}500$ km s^{-1} in more detail than was possible previously. We confirm the long-suspected presence of a void behind the Virgo Cluster core but find that it does not extend to the south; in fact at declinations below 8°, we find very little difference in density between the redshift range 3500–5500 and the southern extension of the Great Wall. For ongoing peculiar velocity studies, we assign these galaxies and others in the window $10^h < \text{R.A.} < 14^h$, $-2° < \text{decl.} < 20°$, $1500 \leq v_\odot \leq 8000$ km s^{-1} to clouds (probably unbound but at a common distance) and subclouds (likely to be virialized).

We have examined separately regions of "high," "medium," and "low" density, particularly to see if there are significant differences in the luminosity functions of those regions. We find no statistically significant differences, nor do we find significant differences in optical surface brightness (averaged over the optical disk). However, our sample selection procedures are not sensitive to galaxies of *very* low surface brightness and therefore we cannot contradict reports that such objects are more abundant in "low-" than in "high-"density regions.

The recent discovery of low-redshift Lyα absorption lines in the spectrum of 3C 273 raises another important question for our sample of galaxies. We investigated the connection between those absorption lines and the large-scale structure of galaxies in the volume behind the southern extension of the Virgo Cluster. The probability of a randomly placed quasar line of sight intersecting an H I disk associated with an optically identified galaxy is approximately 10 times larger in the Local Supercluster redshift range than in either the region between the Local Supercluster and the Great Wall, or the southern extension of the Great Wall itself. This is consistent with the finding of Morris et al. (1993) that the clouds which give rise to the absorptions must be suppressed in high density environments like that of the southern extension of the Virgo Cluster. Also, absorptions are present at Great Wall redshifts while there are none in the space between the two structures, in spite of the near equality of the densities in those two redshift ranges.

In a companion paper we discuss the relationship between the observed absorption lines and the galaxies nearest to the line of sight to the quasar. We shall find there some positive correlations on intermediate and small length scales, in contrast to the large-scale disparities in the previous paragraph. We also postpone conjectures on the physical nature of the absorbers to this companion paper.

M. D. Charles assisted in the preparation of the figures. The referee, G. Gavazzi, contributed comments which have helped us to improve the presentation of this paper. The Arecibo staff was, as always, hospitable, attentive, and helpful throughout these observations. This work was supported in part by US National Science Foundation grants AST87-13394 and AST90-15181 at Lafayette College and by AST90-15451 and AST91-19475 at Cornell, and in part by the National Astronomy and Ionosphere Center which is operated by Cornell University for the National Science Foundation.

REFERENCES

Babul, A., & Rees, M. J. 1992, MNRAS, 255, 346
Bahcall, J. N., Jannuzi, B. T., Schneider, D. P., Hartig, G. F., Bohlin, R., & Junkkarinen, V. 1991, ApJ, 377, L5
Binggeli, B., Popescu, C. C., & Tammann, G. A. 1993, A&ASS, 98, 275 (BPT)
Binggeli, B., Sandage, A., & Tammann, G. A. 1985, AJ, 90, 1681 (BST)
———. 1988, ARA&A, 26, 509
Binggeli, B., Tammann, G. A., & Sandage, A. 1987, AJ, 94, 251
Binggeli, B., Tarenghi, M., & Sandage, A. 1990, A&A, 228, 42
Bothun, G. D., Schombert, J. M., Impey, C. D., Sprayberry, D., & McGaugh, S. S. 1993, AJ, 106, 530
Bottinelli, L., Gouguenheim, L., Fouqué, P., & Paturel, G. 1990, A&AS, 82, 391
Bridle, A. H., Davis, M. M., Fomalont, E. B., & Lequeux, J. 1972, AJ, 77, 405
Briggs, F. H. 1990, AJ, 100, 999
Bushouse, H. A. 1987, ApJ, 320, 49
Dekel, A., & Silk, J. 1986, ApJ, 303, 39
de Lapparent, V., Geller, M. J., & Huchra, J. P. 1989, ApJ, 343, 1
de Vaucouleurs, G., & Corwin, H. G. 1986, AJ, 92, 722
de Vaucouleurs, G., de Vaucouleurs, A., Corwin, H. G., Buta, R. J., Paturel, G., & Fouqué, P. 1991, Third Reference Catalog of Bright Galaxies (New York: Springer) (RC3)
de Vaucouleurs, G., & Peters, W. L. 1985, ApJ, 297, 27
Dickey, J. M., Keller, D. T., Pennington, R., & Salpeter, E. E. 1987, AJ, 93, 788
Dressler, A. 1991, ApJS, 75, 241
Dreyer, J. L. E. 1888, MmRAS, 49, 1 (NGC)
———. 1895, MmRAS, 51, 185 (IC)
———. 1908, MmRAS, 59, 105 (IC)
Eder, J. A., Schombert, J. M., Dekel, A., & Oemler, A. 1989, ApJ, 340, 29
Freudling, W., Haynes, M. P., & Giovanelli, R. 1988, AJ, 96, 1791 (FHG)
Ftaclas, C., Fanelli, M. N., & Strubel, M. F. 1984, ApJ, 282, 19
Fukugita, M., Okamura, S., & Yasuda, N. 1993, ApJ, 412, L13
Garcia, A. M., Bottinelli, L., Garnier, R., Gouguenheim, L., & Paturel, G. 1993, A&ASS, 97, 801
Gavazzi, G. 1987, ApJ, 320, 96
Gavazzi, G., Garilli, B., & Boselli, A. 1990, A&ASS, 82, 399
Gavazzi, G., & Trinchieri, G. 1989, ApJ, 342, 718
Geller, M. J., & Huchra, J. P. 1983, ApJS, 52, 61 (GH)
Gordon, D., & Gottesman, S. T. 1981, AJ, 86, 161
Han, M., & Mould, J. 1990, ApJ, 360, 448
Haynes, M. P., & Giovanelli, R. 1984, AJ, 89, 758
———. 1986, ApJ, 306, 466 (HG)
Helou, G., Giovanardi, C., Salpeter, E. E., & Krumm, N. 1981, ApJS, 46, 267
Helou, G., Hoffman, G. L., & Salpeter, E. E. 1984, ApJS, 55, 433
Hoffman, G. L. 1989, in Large Scale Structure and Motions in the Universe, ed. M. Mezzetti et al. (Dordrecht: Kluwer), 365
Hoffman, G. L., Helou, G., Salpeter, E. E., Glosson, J., & Sandage, A. 1987, ApJS, 63, 247 (HHSGS)
Hoffman, G. L., Helou, G., Salpeter, E. E., & Lewis, B. M. 1989a, ApJ, 339, 812
Hoffman, G. L., Lewis, B. M., Helou, G., Salpeter, E. E., & Williams, H. L. 1989b, ApJS, 69, 65 (HLHSW)
Hoffman, G. L., Lu, N. Y., & Salpeter, E. E. 1992, AJ, 104, 2086
Hoffman, G. L., Williams, H. L., Salpeter, E. E., Sandage, A., & Binggeli, B. 1989c, ApJS, 71, 701
Huchra, J. P., Davis, M., Latham, D., & Tonry, J. 1983, ApJS, 52, 89
Huchtmeier, W. K., & Richter, O.-G. 1989, A General Catalog of H I Observations of Galaxies (New York: Springer)
Humphries, R. M., Pennington, R. L., & Ghigo, F. D. 1987, Visitor Use of the Automated Plate Scanner (University of Minnesota publication) (MAPS)
Iovino, A., Giovanelli, R., Haynes, M., Chincarini, G., & Guzzo, L. 1993, MNRAS, 265, 21
Jerjen, H., & Tammann, G. A. 1993, A&A, 276, 1
Karachentsev, I. D., & Kopylov, A. I. 1990, MNRAS, 243, 390
Kenezek, P. 1993, Ph.D. thesis, Univ. of Massachusetts
Knezek, P. M., & Schneider, S. E. 1993, in The Evolution of Galaxies and Their Environment, ed. D. Hollenbach et al. (NASA Conference Publication 3190) (Moffett Field, CA: NASA), 84
Lacey, C., & Silk, J. 1991, ApJ, 381, 14
Lu, N. Y., Hoffman, G. L., Groff, T., Roos, T., & Lamphier, C. 1993, ApJS, 88, 383
Lu, N. Y., Salpeter, E. E., & Hoffman, G. L. 1994, ApJ, 426, 473

© American Astronomical Society • Provided by the NASA Astrophysics Data System

1995ApJ...441...28H

Lucey, J. R., Guzman, R., Carter, D., & Terlevich, R. J. 1991, MNRAS, 253, 584
Morris, S. L., Weymann, R. J., Dressler, A., McCarthy, P. J., Smith, B. A., Terrile, R. J., Giovanelli, R., & Irwin, M. 1993, ApJ, 419, 524
Morris, S. L., Weymann, R. J., Savage, B. D., & Gilliland, R. L. 1991, ApJ, 377, L21
Nilson, P. 1973, Uppsala General Catalogue of Galaxies (Uppsala Astr. Obs. Ann., 6) (UGC)
Nolthenius, R., & White, S. D. M. 1987, MNRAS, 225, 505
Odewahn, S. C., Stockwell, E. B., Pennington, R. L., Humphreys, R. M., & Zumach, W. A. 1992, AJ, 103, 318
Pellegrini, P. S., & da Costa, L. N. 1990, ApJ, 357, 408
Ramella, M., Geller, M. J., & Huchra, J. P. 1992, ApJ, 384, 396
Salpeter, E. E. 1993, AJ, 106, 1265
Salpeter, E. E., & Hoffman, G. L. 1995, ApJ, 441, 51
Salzer, J. J. 1992, AJ, 103, 385
Salzer, J. J., Hanson, M. M., & Gavazzi, G. 1990, ApJ, 353, 39
Sandage, A., & Tammann, G. A. 1990, ApJ, 365, 1
Schombert, J. M., Bothun, G. D., Schneider, S. E., & McGaugh, S. S. 1992, AJ, 103, 1107
Schneider, S. E., Helou, G., Salpeter, E. E., & Terzian, Y. 1986, AJ, 92, 742
Shimasaku, K., & Okamura, S. 1992, ApJ, 398, 441
Sulentic, J. W., & Arp, H. 1983, AJ, 88, 489
Tanaka, K. 1985a, PASJ, 37, 133
———. 1985b, PASJ, 37, 427
Teerikorpi, P., Bottinelli, L., Gouguenheim, L., & Paturel, G. 1992, A&A, 260, 17
Thompson, L. A., & Gregory, S. A. 1993, AJ, 106, 2197
Tully, R. B. 1987, ApJ, 321, 280
Tully, R. B., & Shaya, E. 1984, ApJ, 281, 31
Tully, R. B., Shaya, E., & Pierce, M. J. 1992, ApJSS, 80, 479
Tyson, N. D., & Scalo, J. M. 1988, ApJ, 329, 618
van Gorkom, J. 1993, in The Environment and Evolution of Galaxies, ed. J. M. Shull & H. A. Thronson (Dordrecht: Kluwer), 345
van Gorkom, J. H., Bahcall, J. N., Jannuzi, B. T., & Schneider, D. P. 1993, AJ, 106, 2213
Weinberg, D. H., Szomoru, A., Guhathakurta, P., & van Gorkom, J. H. 1991, ApJ, 372, L13
Williams, B., & Kerr, F. 1981, AJ, 86, 953 (WK)
Zwicky, F., Herzog, E., & Wild, P. 1961–1963, Catalogue of Galaxies and Clusters of Galaxies (Pasadena: California Inst. of Technology) (CGCG)

© American Astronomical Society • Provided by the NASA Astrophysics Data System